DC-1721

ORNL-5082

# Controlled Thermonuclear Materials Technology Program Annual Progress Report for Period Ending June 30, 1975



OAK RIDGE NATIONAL LABORATORY

operated by Union Carbide Corporation • for the U.S. Atomic Energy Commission

BLANK PAGE

Printed in the United States of America. Available from
National Technical Information Service
U.S. Department of Commerce
5285 Port Royal Road, Springfield, Virginia 22161
Price: Printed Copy $5.45; Microfiche $2.25

ORNL-5082
UC-20 – Controlled
Thermonuclear
Processes and
Plasma Physics

Contract No. W-7405-eng-26

METALS AND CERAMICS DIVISION

# CONTROLLED THERMONUCLEAR MATERIALS TECHNOLOGY PROGRAM ANNUAL PROGRESS REPORT FOR PERIOD ENDING JUNE 30, 1975

Compiled by J. L. Scott

Manager, Controlled Thermonuclear Research Materials

Edited by Sigfred Peterson

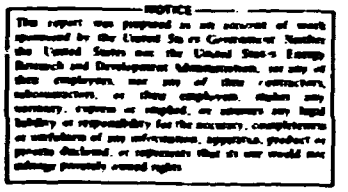


OCTOBER 1975

OAK RIDGE NATIONAL LABORATORY
Oak Ridge, Tennessee 37830
operated by
UNION CARBIDE CORPORATION
for the
U.S. ENERGY RESEARCH AND DEVELOPMENT ADMINISTRATION

CONTENTS

BLANK PAGE

## FOREWORD

The Controlled Thermonuclear Research (CTR) Program in the Metals and Ceramics Division, which is described in this report, is directed toward solving the materials problems of the Thermonuclear Division of ORNL and in meeting the needs of the national CTR program, directed by the ERDA Division of Controlled Thermonuclear Research. The Thermonuclear Division, directed by J. F. Clarke with O. B. Morgan, Jr. as Associate Director consists of seven departments, listed below with the respective department head:

| | | |
|---|---|---|
| I. | High Beta Plasma Department | R. A. Dandl |
| II. | Low Beta Plasma Department | L. A. Berry |
| III. | Plasma Theory Department | G. E. Guest |
| IV. | Plasma Heating Department | L. D. Stewart |
| V. | Advanced Systems Department | M. Roberts |
| VI. | Engineering Sciences Department | H. M. Long |
| VII. | Fusion Reactor Technology Department | D. Steiner |

Except for the Plasma Theory Department, all the Departments listed above have materials problems that require attention now or will in the future.

A major objective of the CTR program at ORNL is the development of TOKAMAK systems. In a TOKAMAK, the plasma is magnetically confined by toroidal field magnets and a poloidal field created by inducing an electric current in the plasma. The electric current also heats the plasma up to average ion energies of about 1 keV, but about 10 keV is necessary to initiate a self-sustained thermonuclear reaction in a deuterium-tritium (D-T) fueled system. Auxiliary heating methods being pursued at ORNL include the injection of energetic (25–150 keV) neutral beams of deuterium and microwave heating. A detailed description of the ORNL reference commercial TOKAMAK has been published.[1]

If the D-T thermonuclear reaction can be effected, the products are 3.5 MeV alpha particles, which heat the plasma, and 14.1 MeV neutrons, which enter the blanket. Severe radiation damage is expected as a result

---

[1] A. P. Fraas, *Conceptual Design of the Blanket and Shield Region and Related Systems for a Full Scale Toroidal Fusion Reactor*, ORNL-TM-3096 (May 1973).

BLANK PAGE

of the high neutron fluences envisioned. Therefore, a high-priority goal of the fusion program is to develop a structural wall for the blanket. Since tritium is not found in nature, but must be produced from lithium, the blanket will contain some form of lithium, either liquid metal, fused salt, or solid compound. The structural wall must be compatible with the lithium-bearing material. The heat deposited in the blanket from the plasma and from the neutrons must be removed and converted to electrical energy by a reasonably efficient thermodynamic cycle. Therefore, a coolant is required that can remove heat efficiently in an intense magnetic field. The coolant must also be compatible with the structural walls and the lithium-bearing materials. Finally, the tritium generated in the lithium must be removed and processed without adverse environmental effects. The numerous complex problems associated with blanket development come under the purview of the Fusion Reactor Technology Department, directed by D. Steiner. Within the Metals and Ceramics Division, the bulk radiation effects program and the compatibility program are in this category.

Superconducting magents are required to create the intense toroidal magnetic field without excessive power losses. The superconducting magnets are being developed in the Engineering Sciences Department under H. M. Long. The Metals and Ceramics Division supports the effort with studies of the effects of stress on conductors, the development of fabrication techniques and quality assurance programs for conductor manufacture, and a study of the eddy currents in the toroidal field coils arising from the presence of the ohmic heating and vertical field coils.

One of the major problems associated with achieving the thermonuclear plasmas is the presence of impurities in the plasma. The impurities result in both line radiation losses and bremstrahlung losses proportional to about the fourth power of the atomic number. The impurities arise from contaminants on the surfaces of the plasma confinement system and from atoms sputtered off the first wall. The effects of impurities are being studied in ORMAK, the Oak Ridge TOKOMAK, by the Low Beta Plasma Department, under the direction of L. A. Berry. In the Metals and Ceramics Division, surface analyses have been made of the ORMAK liner and techniques developed for cleaning the liner and for *in-situ* diagnostics of TOKAMAK liners.

The research-scale studies on the TOKAMAK system have been sufficiently successful that efforts are being made to design an Experimental Power Reactor and subsequently a Demonstration Reactor. These efforts are directed by M. Roberts, head of the Advanced Systems Department. Numerous materials problems relating to materials selection and evaluation of performance necessarily arise in these design studies. A small group in the Metals and Ceramics Division is participating in the effort.

This report contains a summary description of the materials work done in FY 1975 for the CTR program.

# SUMMARY

## 1. RADIATION EFFECTS

The high helium production rates expected in fusion reactors can be simulated in alloys containing nickel by irradiation in a thermal reactor. Results are reported of specimens irradiated in HFIR to exposures equivalent to six years of displacement damage and 20 years of helium production at a neutronic wall loading of 1 $MW/m^2$. Large amounts of helium greatly increase cavity concentrations but only slightly increase cavity sizes. An analysis of the cavity distributions and helium contents indicates that the cavities are near-equilibrium bubbles with the amount of void character increasing with decreasing irradiation temperature. Recovery, recrystallization, and precipitation were all enhanced by irradiation. An analysis of swelling and uniform strain of stainless steel indicates that 20%-cold-worked type 316 stainless steel can be used as a first-wall constructional material with an expected lifetime of at least five years (50 dpa and 1000 at. ppm He) for design temperatures not exceeding 550°C. Electron microscopy and mechanical properties measurements on V–20% Ti irradiated in EBR-II to fluences between 0.5 and $6.1 \times 10^{22}$ $n/cm^2$ at temperatures ranging from 370 to 805°C showed no swelling or significant loss in ductility. Voids were found in V–10% Cr and VANSTAR-7. A heavy charged-particle recoil data base along with an analysis program has been created to provide assistance in studying, evaluating, and correlating radiation effects. Gas production and nuclear displacements for most of the elements of interest to the CTR program are included for all neutron reactions for which cross sections are available from ENDF/B-IV. The status of neutron irradiation experiments is summarized.

## 2. SURFACE STUDIES

In laboratory studies oxygen glow discharge cleaning removed essentially all the carbon present on the surface of samples of the ORMAK liner. Such cleaning techniques, now routine in ORMAK operations, result in significantly higher plasma currents. A soft x-ray appearance potential spectrometer has been designed, tested, and installed on ORMAK, and preliminary data are being obtained. A new surface research facility is being established for the studies necessary to select and test advanced wall materials. This facility will be used initially to perfect techniques for quantative analysis of liner materials in present and future TOKAMAK devices.

## 3. COMPATIBILITY STUDIES

An extensive literature search was completed on the compatibility relationships between lithium and various iron-base alloys, and the results of this search were used to plan and initiate a detailed compatibility program. Analysis was completed on a test designed to determine the partitioning of oxygen between niobium or Nb–1% Zr and lithium with

BLANK PAGE

with $Al_2O_3$ contacting the side of the metal away from the lithium. Work was initiated to develop techniques and determine the effectiveness of impregnating reactor-grade graphite with lithium-bearing compounds. A type 316 stainless steel thermal-convection loop has been fabricated and will be used to determine the effects of composition deviations in $Li_2BeF_4$ on the oxidation potential of the salt.

## 4. MAGNET DEVELOPMENT

Mockup extrusion billets were designed and assembled to evaluate methods for stacking to achieve the best packing density. Billets were assembled containing niobium-titanium stacking elements and several randomly distributed thermocouples to monitor heating before extrusion. Billets were assembled and extruded to wirebar and subsequently drawn to 0.015-in.-diam (0.38-mm) wire. Thermal tabs were used in a few billets in an effort to better understand and define the thermal profile of the extruded wirebar.

Niobium-titanium alloys ranging in composition from 45 to 55 wt % Ti are under consideration as the filaments in copper-base superconductive wire for fusion reactor magnets. An important aspect of the performance capability is the quality of this material with respect to chemical composition and metallurgical integrity. Therefore, control of these features must be established before manufacture of the superconductive wire. This control is established at a product form consisting of a rod 0.5 in. (13 mm) in diameter for alloys containing 45 wt % Ti and 48 wt % Ti by ORNL specifications identified as ORNL-TD-SC-1 and ORNL-TD-SC-2, respectively. Nearly 4000 lb (1800 kg) of these alloys has been procured for the current ORNL programs to the requirements of these specifications.

Lots of the Nb–45 wt % Ti alloy produced by Teledyne Wah Chang Albany and Kawecki-Berylco were tested for composition, variations in the composition, and metallurgical properties. At this stage of processing, where the material is in the form of 0.5-in.-diam (13-mm) rods, the most distinctive characteristic is a "coring" effect, which appears related to chemical inhomogeneity of titanium, and the presence of a grain boundary precipitate of eutectic structure, especially noticeable in the Wah Chang material. Variations in composition do not appear to be significant. For example, statistically it can be shown that in the Wah Chang lot of 205 rods, 99.7% of these rods would comply with the titanium concentration requirement of 45 ± 2 wt %. The noticeable differences between the Wah Chang material and the Kawecki-Berylco material were the higher values in the reduction of area of the Kawecki-Berylco rods, the higher concentration of zirconium and tin as tramp impurities in the Wah Chang rods, and the more extensive grain boundary precipitate in the Wah Chang rods.

Pseudoelastic behavior and serrated stress-strain curves have been found both in superconducting composites and niobium-titanium alloys at 4.2 K. The exact mechanisms of these effects are not clear at this time, although a reversible stress-induced martensitic transformation in the niobium-titanium could be occurring. Both these effects could result in

rather large temperature increases and could have adverse effects on the superconducting behavior of the conductor. The degree of the effects, which originate in the Nb-Ti, depend critically on the composite geometry. Differences in tensile behavior were found in composites with straight filaments compared with those with twisted filaments. A possible explanation is that the twisted filaments have a "spring" action and do not act upon the matrix in the same manner as straight filaments. As a first approximation, the rule of mixtures seems to be useful in predicting the tensile properties.

Equations and scaling laws have been derived to calculate the forces and heating effects produced by changing currents in a coil in the presence of other coils and conductors. Analytic solutions can be obtained for symmetric configurations, and relaxation or iterative solutions are used for more complicated geometries. A third approach is to use the derived scaling laws in connection with measurements on models.

## 5. EPR DESIGN SUPPORT

Materials support was provided for the EPR design study. The structural material selected for the blanket is 20%-cold-worked type 316 stainless steel. The operating temperature is limited to a maximum of 550°C both by radiation-induced swelling and loss of ductility and by compatibility with lithium. Since type 316 stainless steel is not likely to be the material most resistant to sputtering induced by the plasma, a liner is recommended for the EPR. An experimental program is required to identify the best liner material.

## 6. THE INFLUENCE OF STRUCTURAL MATERIALS ON FUSION-REACTOR-BLANKET RESPONSE

The effects on nuclear response functionals (i.e., tritium breeding ratio, energy deposition, absorbed dose during operation, material activation, activation dose after shutdown, and radiation damage) are calculated when niobium, type 304 stainless steel, and Nimonic 105 are considered as the structural materials in the ORNL conceptual reactor design. No gross differences among the three structural materials are found; however, type 304 stainless steel appears to be the best choice since it is more readily available.

# 1. RADIATION EFFECTS

J. O. Stiegler E. E. Bloom

## 1.1 MICROSTRUCTURE OF IRRADIATED TYPE 316 STAINLESS STEEL CONTAINING HIGH HELIUM CONCENTRATIONS — J. P. Maziasz

### 1.1.1 Purpose

The purpose of this investigation is to determine the effects of high helium contents and irradiation on the microstructure of both 20%-cold-worked and solution-annealed type 316 stainless steel. These data, when correlated with swelling and mechanical properties measurements, should help determine possible operating conditions for a fusion reactor first wall made of type 316 stainless steel. This report describes the effect of irradiation temperature at nearly constant gas content and dpa or dose level. Specimens were irradiated in the High Flux Isotope Reactor (HFIR), where helium was generated by the two-step reaction of $^{58}Ni$ with thermal neutrons. Exposures were equivalent to up to six years of displacement damage and 20 years of helium production in a fusion reactor at a wall loading of 1 $MW/m^2$.

### 1.1.2 Experimental Description

Only a brief description of the experiment will be given here; detailed accounts can be found in previous publications.[1,2] The stainless steel tensile specimens were prepared from rod stock of the following composition:

| Fe | Cr | Ni | Mo | Mn | Ti | Si | C | P | S | N | B |
|---|---|---|---|---|---|---|---|---|---|---|---|
| 63.6 | 18.0 | 13.0 | 2.58 | 1.9 | 0.05 | 0.8 | 0.05 | 0.013 | 0.016 | 0.05 | 0.0005 |

These values are averages of multiple determinations on the same heat.

---

[1] F. W. Wiffen and E. E. Bloom, *Effect of High Helium Content on Stainless Steel Swelling*, ORNL-TM-4541 (May 1974).

[2] E. E. Bloom and F. W. Wiffen, *The Effects of Large Concentrations of Helium on the Mechanical Properties of Neutron-Irradiated Stainless Steel*, ORNL-TM-4861 (May 1975).

BLANK PAGE

The samples were solution treated at 1050°C for 1 hr to produce an average grain size of about 50 μm; part of the specimens were then cold worked to a 20% reduction of area by swaging. Tensile specimens of gage length 0.72 in., total length 1.25 in., and gage diameter of 0.08 in. (18.3 by 31.8 by 2.0 mm) were machined from rod stock. They were irradiated in the outer position of the HFIR flux trap, and irradiation temperatures above the coolant temperature (55°C) were attained by a helium-filled gas gap. Irradiation temperatures ranged from 350 to 700°C and the fluences up to $8.7 \times 10^{22}$ n/cm$^2$ (>0.1 MeV). Helium was produced in the samples by a two-step nuclear reaction with thermal neutrons: $^{58}Ni(n,\gamma)^{59}Ni$ followed by $^{59}Ni(n,\alpha)^{56}Fe$.

Disks for electron microscopy were cut from the gage sections of tensile specimens after testing at or near the estimated irradiation temperatures. The cavity populations within the grains are not believed to be altered by the testing procedure, but dislocation structures and densities and grain boundary cavity observations, particularly those for specimens tested above 550°C, may have been modified. Details of the technique for preparing the specimens for transmission electron microscopy have been given previously.[3]

There are discrepancies between dpa levels and helium contents given in this report from those published earlier.[1,2] The dpa values given here are a revision of earlier estimates using the procedure recommended by the IAEA Working Group on Reactor Radiation Measurements.[4] Helium contents are based on more extensive analyses of specimens contained in this experiment.

---

[3]F. W. Wiffen, P. J. Maziasz, J. T. Houston, and E. E. Bloom, "Effects of High-Helium-Generation Rates on Radiation Damage in Stainless Steels," *Semi-Annual Progress Report on Irradiation Effects on Reactor Structural Materials August, 1974 to February, 1975*, HEDL-TME-75-23, pp. ORNL-19–28.

[4]D. G. Doran, et al., *Report of the Working Group on Displacement Models and Procedures for Damage Calculations*, HEDL-TME-73-76 (December 1973).

### 1.1.3 Results

#### 1.1.3.1 Cavity Structures

The cavity concentrations and sizes followed the qualitative trends found in fast-reactor irradiations, namely decreasing concentrations and increasing sizes with increasing irradiation temperature. Results are summarized in Table 1.1. A significant exception was the occurrence of bimodal size distributions in several of the specimens. In the table the figures given in parentheses refer to the larger component of the size distribution, which was present in concentrations two to four orders of magnitude less than the smaller component. For the lower irradiation temperatures (550°C and below) the larger cavities were within the grains, either attached to precipitate particles in annealed material or located near stacking fault bands. For irradiation at 680°C the larger cavities were found on the grain boundaries. A series of photomicrographs illustrating the cavity and precipitate structures is shown in Figs. 1.1 through 1.6. Although data for the annealed samples are limited, cold working apparently increases the cavity concentrations and reduces cavity sizes at temperatures where the structure introduced by cold working is stable (550°C and below). This has the net effect of decreasing the swelling.[1]

For annealed material at 550°C and below and cold-worked material at 450°C and below, the grain boundaries were free of large cavities (see Figs. 1.7 and 1.8), although the annealed material contained almost continuous distributions of precipitate particles. At higher irradiation temperatures the subgrain boundaries and grain boundaries were populated by large, closely spaced cavities (Figs. 1.4–1.6). Regions 0.2 to 2 μm wide adjacent to the boundaries were denuded of cavities, the larger denuded zones being associated with the larger cavities.

For the cold-worked material irradiated at 380°C small cavities were distributed fairly uniformly within the grains, although on a local scale significant size variations were evident, as shown in Fig. 1.1. At higher temperatures cavities were often associated with precipitate particles, but cavity concentrations in all materials were much higher than concentrations of precipitate particles, so the association was not general.

Table 1.1. Microstructural Data on Irradiated Samples

| Condition | Irradiation Temperature (°C) | Neutron Fluence, > 0.1 MeV ($n/cm^2$) | dpa | $\Delta\rho/\rho$[a] (%) | Void Volume[b] Fraction (%) | Cavity Concentration[c] ($cm^{-3}$) | Diameter[c] (Å) |
|---|---|---|---|---|---|---|---|
| Annealed 1 hr at 1050°C | 550 | $6.18 \times 10^{22}$ | 42 | d | 8.5 ± 1.6 | $4.4 \pm 1.3 \times 10^{14}$ ($1.4 \times 10^{12}$) | 500 (3400) |
| | 680 | 8.74 | 60 | 14.1 | d | d | d |
| 20% Cold Worked After 1 hr at 1050°C | 380 | 7.05 | 48 | 1.6 | 2.2 ± 0.4 | $1.8 \pm 0.4 \times 10^{16}$ ($4.5 \times 10^{12}$) | 95 (1100) |
| | 450 | 7.69 | 53 | 0.80 | 2.0 ± 0.4 | $6.6 \pm 1.6 \times 10^{15}$ | 170 |
| | 550 | 6.18 | 42 | d | d | d | d |
| | 600 | 8.71 | 60 | 3.3 | 2.9 ± 1.4 | $3.4 \pm 2.7 \times 10^{14}$ | 450 |
| | 680 | 8.74 | 60 | 16.8 | 16.8 ± 3.6 | $6.3 \pm 2.6 \times 10^{13}$ ($1.4 \times 10^{12}$) | 1100 (7100) |

[a]Obtained from immersion density measurements.

[b]Obtained from electron micrographs.

[c]The numbers in parentheses are for the large portion of the bimodal distribution observed.

[d]Not available.

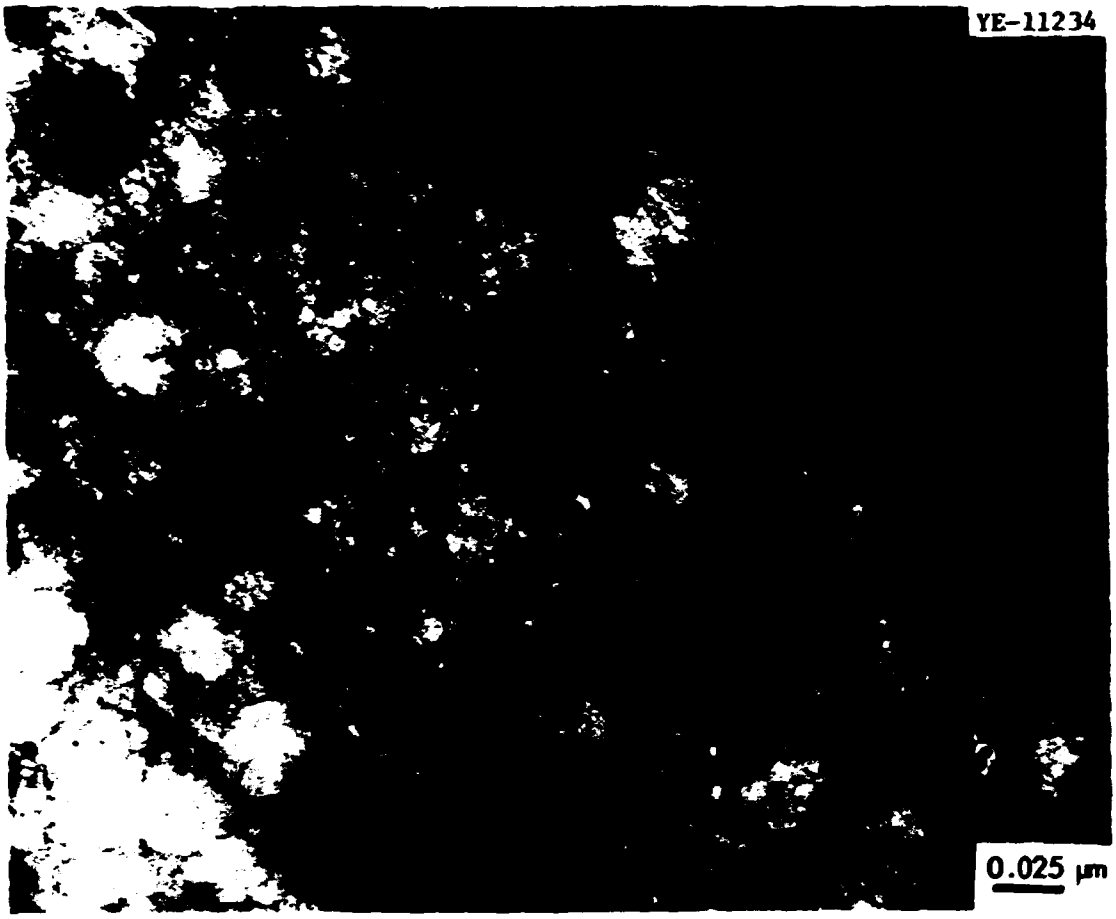


Fig. 1.1. Type 316 Stainless Steel, 20% Cold Worked, Irradiated at 380°C to 48 dpa and 3400 ppm He. This micrograph shows the variation in cavity sizes that occurs on a local level. The small cavities pictured here are fairly uniformly distributed. A few very large cavities were found associated with stacking fault bands.

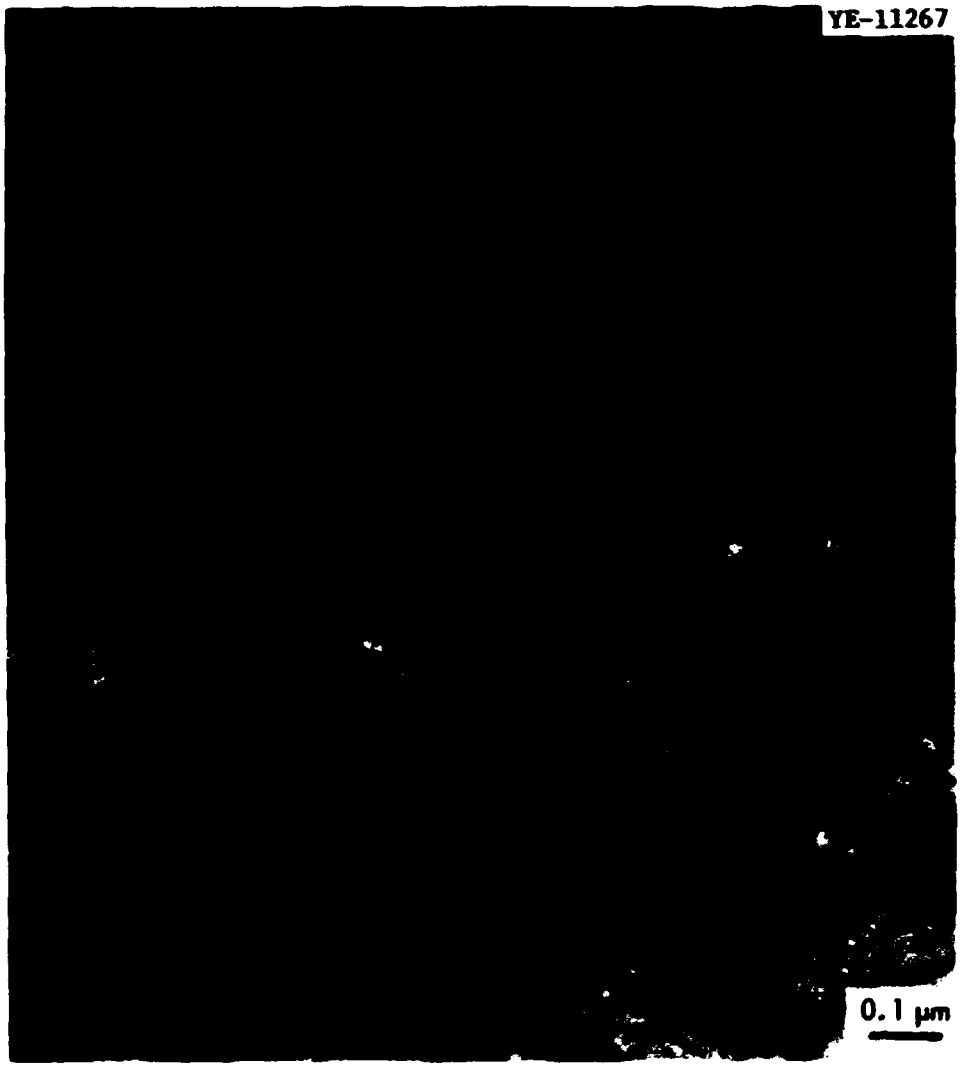


Fig. 1.2. Type 316 Stainless Steel, 20% Cold Worked, Irradiated at 550°C to 42 dpa and 2950 ppm He.


Fig. 1.3. Type 316 Stainless Steel, 20% Cold Worked, Irradiated at 600°C to 60 dpa and 4150 ppm He. This picture is typical of a recently recrystallized region. Also, note the lack of precipitate particles in grains.

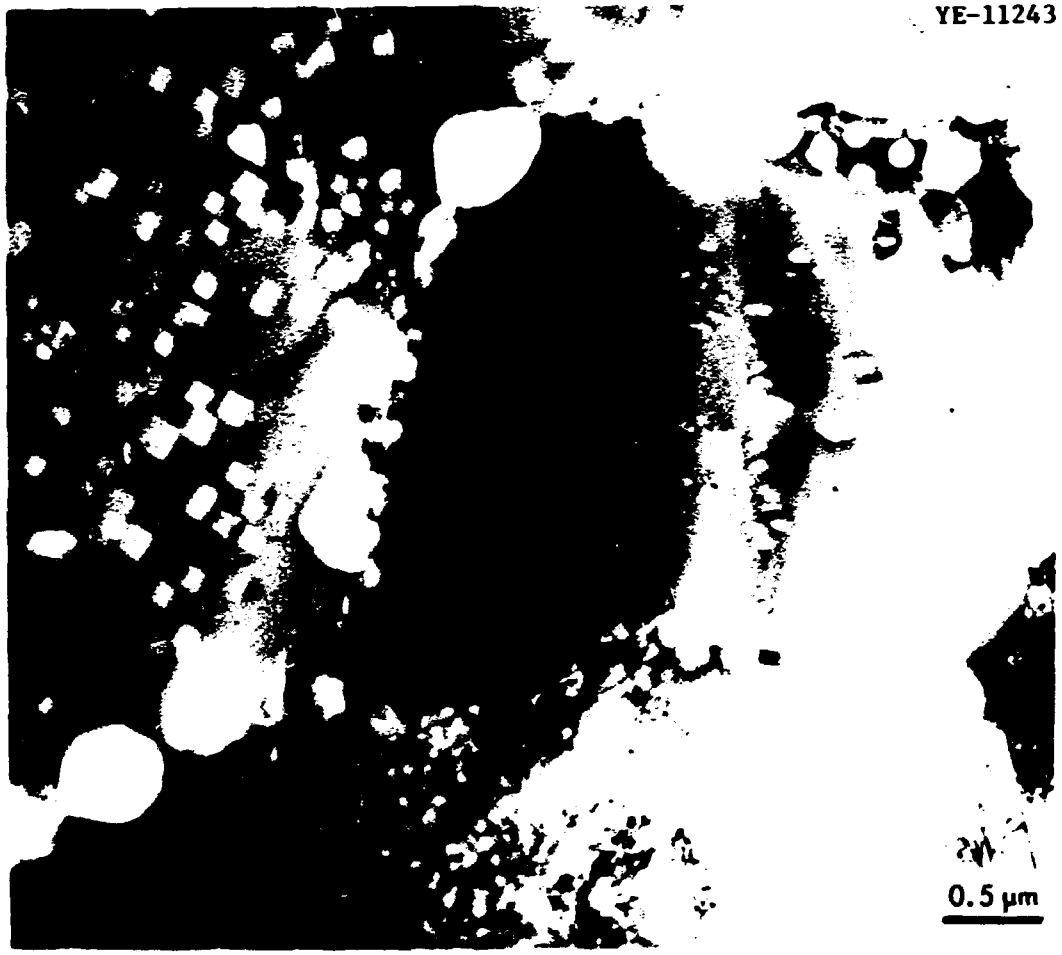


Fig. 1.4. Type 316 Stainless Steel, 20% Cold Worked, Irradiated at 680°C to 60 dpa and 4240 ppm He. This micrograph shows a large sigma phase region at a grain junction and very large cavities at grain boundary and grain-precipitate interfaces. Note the flat cavities in the sigma phase.

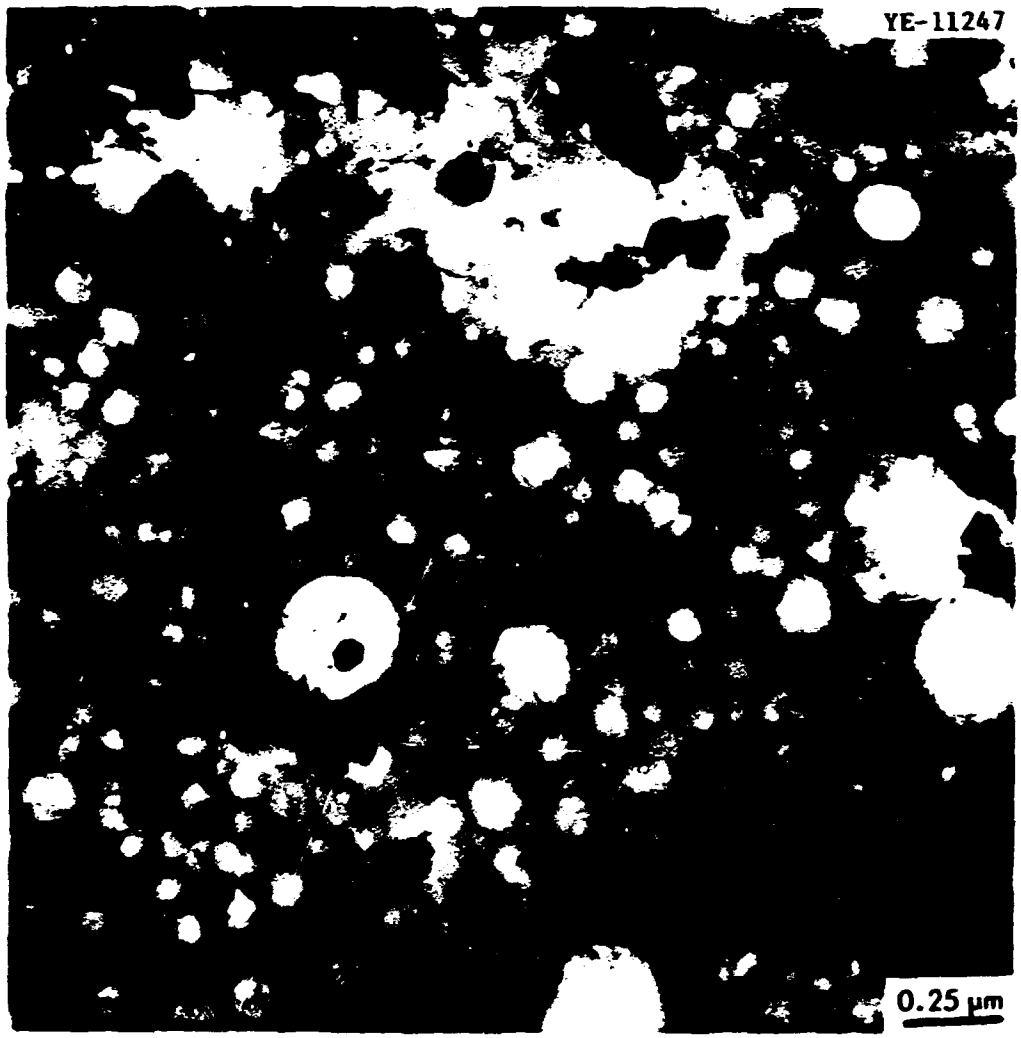


Fig. 1.5. Type 316 Stainless Steel Solution Annealed for 1 hr at 1050°C, Irradiated at 550°C to 42 dpa and 2950 ppm He.

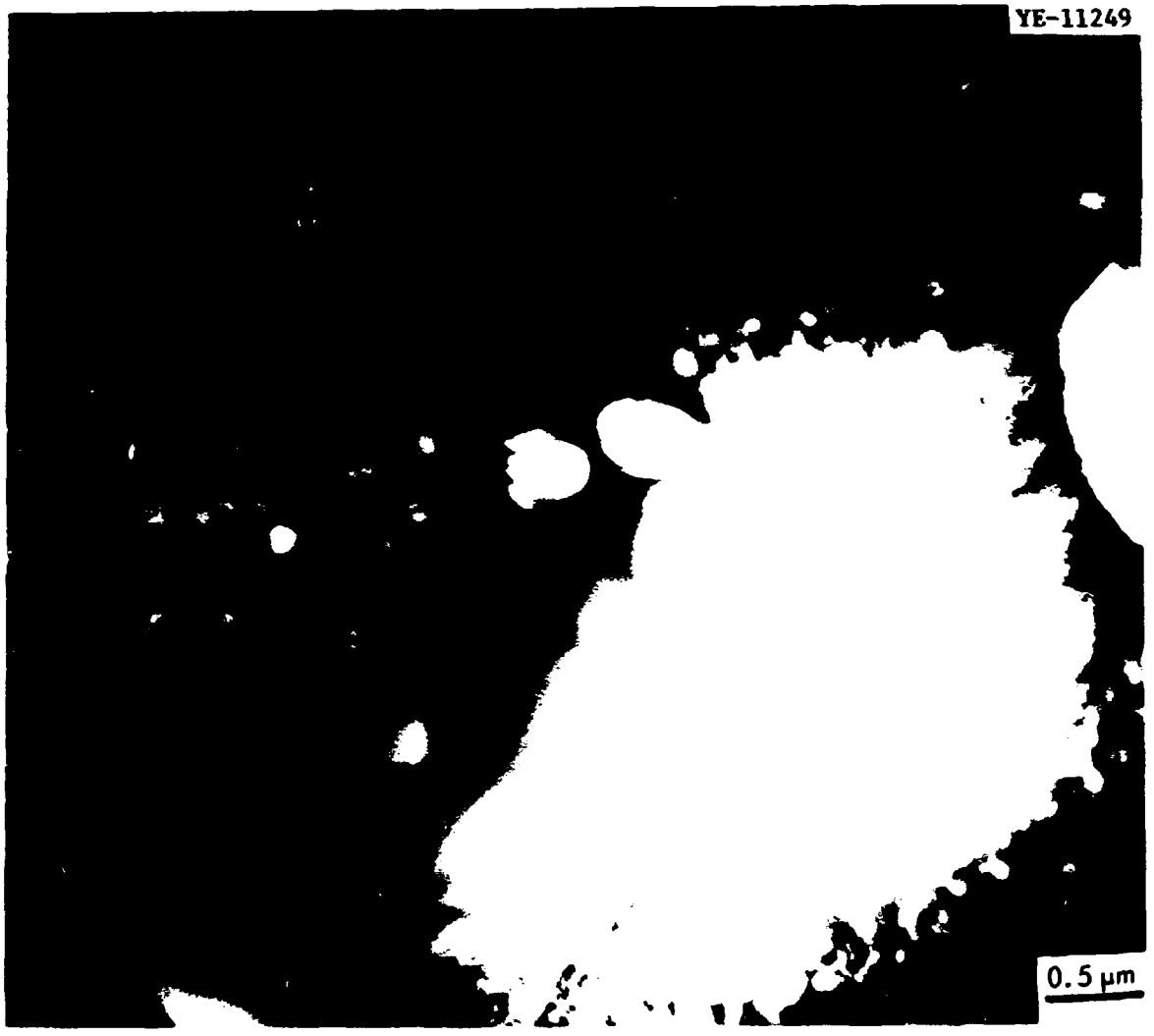


Fig. 1.6. Type 316 Stainless Steel Solution Annealed for 1 hr at 1050°C, Irradiated at 680°C to 60 dpa and 4240 ppm He. Shows large sigma phase with flat cavities and large cavities at the grain boundary and at grain-precipitate interface. Very similar to cold worked-sample for the same irradiation conditions (Fig. 1.4).

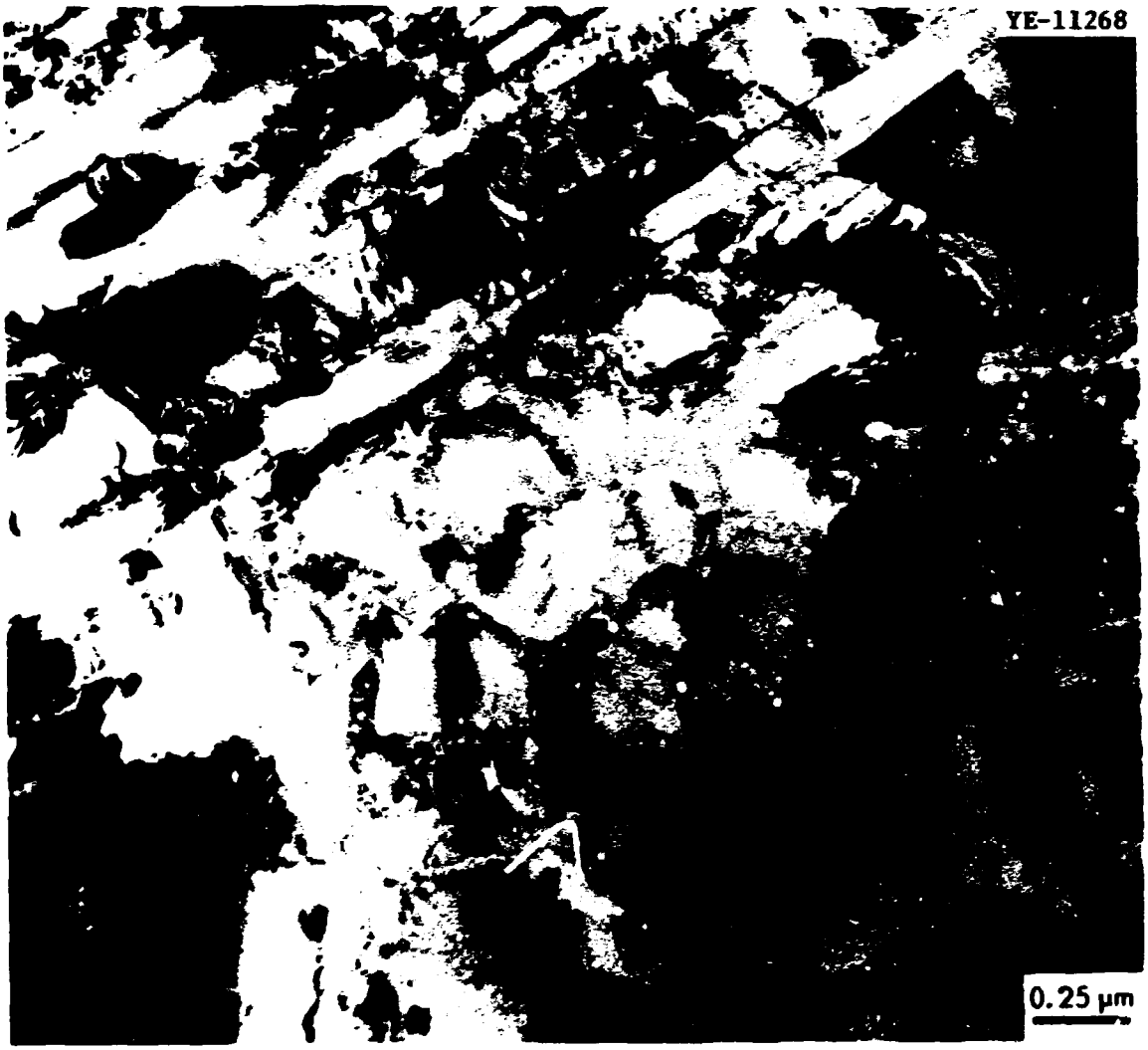


Fig. 1.7. 20% Cold Worked, Irradiated at 550°C to 42 dpa and 2950 ppm He. A grain boundary region — note the large sigma phase particles at the grain boundary and cavities that are slightly larger than those in the matrix.

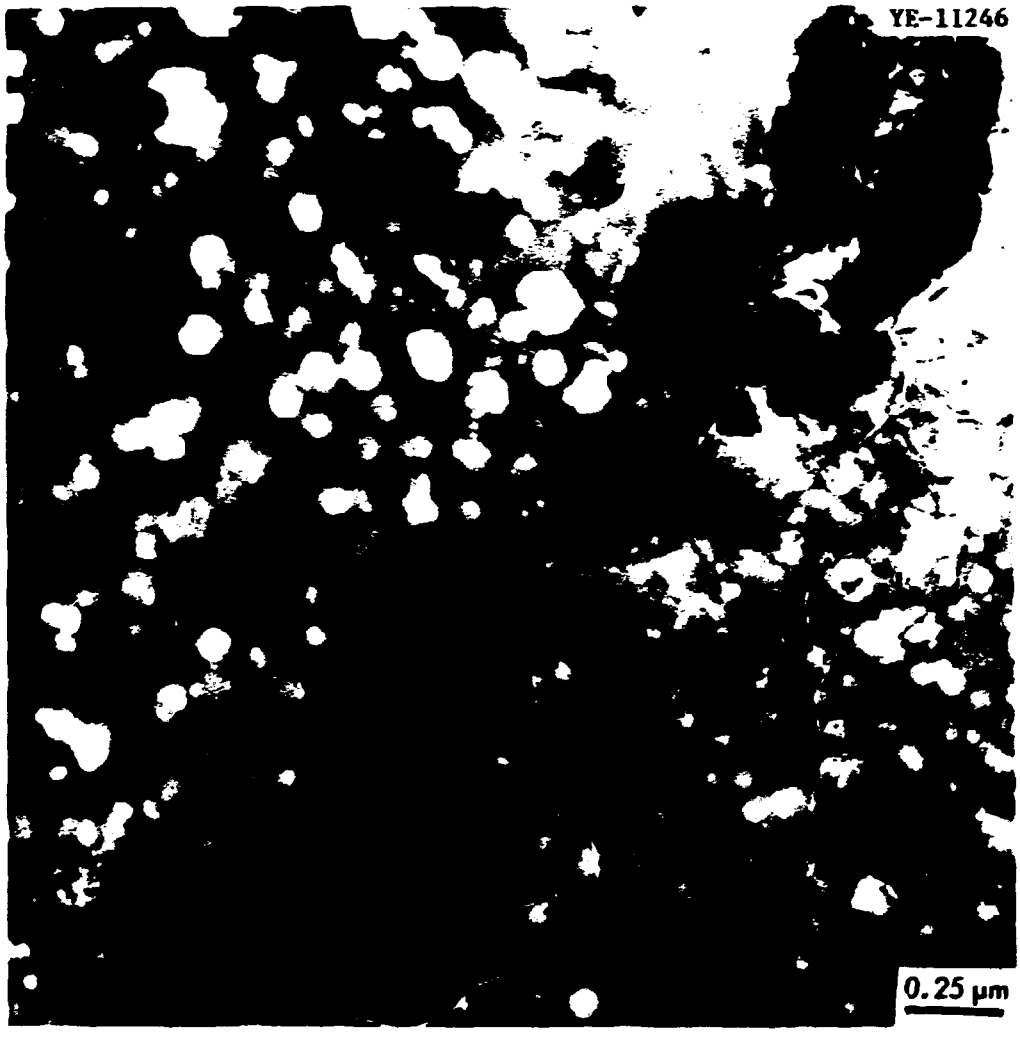


Fig. 1.8. Type 316 Stainless Steel Solution Annealed for 1 hr at 1050°C, Irradiated at 550°C to 42 dpa and 2950 ppm He. Grain boundary regions. Note blocky precipitate at boundary and high concentration of small cavities at precipitate. Note the absence of large cavities from grain boundary region but the presence of small cavities in the precipitate particles.

1.1.3.2 Recovery, Recrystallization, and Precipitation

For specimens irradiated at 550°C and below the higher dislocation density introduced by cold working was retained to the neutron exposures considered here. During the irradiation of about 16,000 hr at 600°C, general recovery into a cell structure occurred. This was considerably enhanced by the irradiation, as only slight recovery of the dislocation structure occurred in 10,000-hr out-of-reactor aging studies at 650°C (Fig. 1.9, compare with Fig. 1.3). Significant recrystallization occurred at 680°C in the reactor where large grains free of substructure were found.


Fig. 1.9. Type 316 Stainless Steel, 20% Cold Worked and Aged at 650°C for 10,000 hr. Compare with Fig. 1.3 taken of a specimen irradiated at 600°C for 16,000 hr.

Precipitation reactions were also enhanced by irradiation. The lowest temperature at which precipitation was observed by electron microscopy in the cold-worked materials was 450°C where it took the form of platelike particles probably oriented along stacking fault bands (Fig. 1.10). Although quantitative measurements are not yet available, the amount is comparable with that occurring in out-of-reactor aging at 650°C (Fig. 1.9). Sigma phase was formed both in and out of the reactor


Fig. 1.10. Type 316 Stainless Steel, 20% Cold Worked, Irradiated at 450°C to 53 dpa and 3810 ppm He. This micrograph shows long as well as small chunky precipitate particles and the cavities in the grain. The grain boundary passing through the center shows only a few precipitate particles and no large cavities.

for temperatures above 600°C. Amounts were larger and particles more massive in the neutron-irradiated materials.[5]

Extensive precipitation occurred within the grains and along the grain boundaries in both annealed and cold-worked specimens irradiated at 550°C. The identity of the particles has not yet been established, but amounts and morphologies differ from those in thermal controls.

### 1.1.3.3 Comparison of HFIR and EBR-II Irradiations

Specimens of this same heat of stainless steel have been irradiated in EBR-II to comparable exposures as part of the LMFBR cladding development program. A comparison of microstructures for materials irradiated to fluences near $6 \times 10^{22}$ n/cm$^2$ (>0.1 MeV) at about 550°C is given in Fig. 1.11. Displacement levels are nearly equal for the two irradiations, but because of the thermal flux in HFIR, helium levels differ greatly (15 ppm in EBR-II vs 3000 ppm in HFIR). This is reflected in the micrographs, where the high helium level in HFIR has significantly increased void concentrations and to a lesser extent increased cavity sizes.

### 1.1.3.4 Nature of the Cavities

Because of the large amounts of helium in the specimens irradiated in HFIR the question naturally arises as to whether the cavities are bubbles or voids. For the cavity concentrations and size distributions reported here we have calculated the amount of helium required to stabilize them as equilibrium bubbles, assuming van der Waals' gas law and taking the specific surface energy to be 1500 ergs/cm$^2$ (1.5 J/m$^2$). Results are given in Table 1.2. The last column, the ratio of measured helium to the required equilibrium helium contents, is a measure of the bubble character of the cavities. A value of 1.0 indicates equilibrium helium bubbles.

Values are all less than 1. At lower temperatures the discrepancy is larger and probably outside uncertainties in the evaluation. The cavities are probably all near-equilibrium bubbles, but at the lower

---

[5]E. E. Bloom and F. W. Wiffen, *The Effects of Large Concentrations of Helium on the Mechanical Properties of Neutron-Irradiated Stainless Steel*, ORNL-TM-4861 (May 1975).

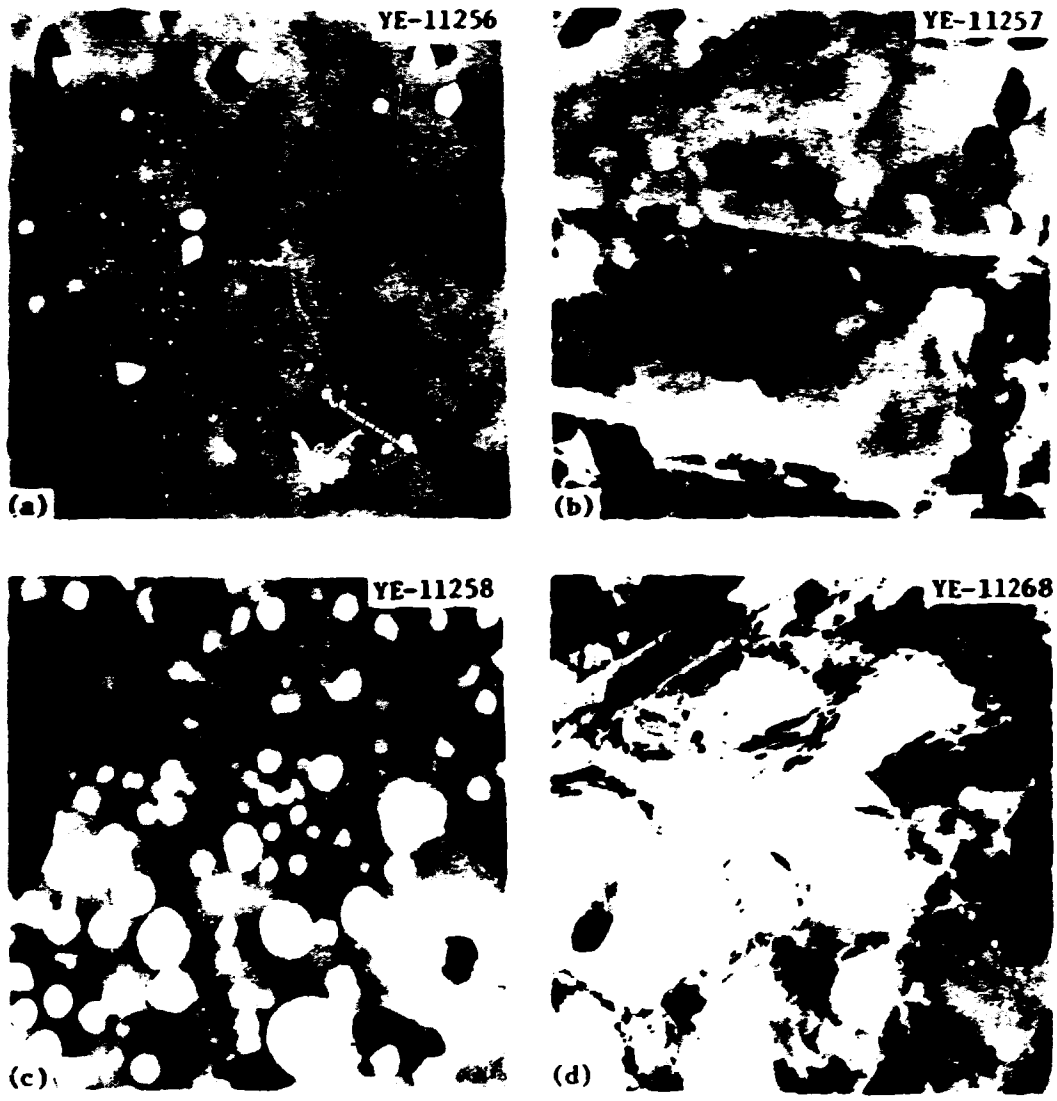


Fig. 1.11. Comparison of Cavity Structures in Type 316 Stainless Steel Irradiated in HFIR (≈3000 ppm He) and EBR-II (≈15 ppm He). 50,000×.
(a) Solution annealed, $5.6 \times 10^{22}$ n/cm$^2$ (35 dpa) at 500–535°C in EBR-II.
(b) 20% cold worked, $5.6 \times 10^{22}$ n/cm$^2$ (35 dpa) at 500–535°C in EBR-II.
(c) Solution annealed, $6.2 \times 10^{22}$ n/cm$^2$ (42 dpa) at 550°C in HFIR.
(d) 20% cold worked, $6.2 \times 10^{22}$ n/cm$^2$ (42 dpa) at 550°C in HFIR.

Table 1.2. Helium Analysis in Irradiated Samples

| Condition | Irradiation Temperature (°C) | Helium Content (at. ppm) | | Measured |
|---|---|---|---|---|
| | | Measured | Calculated for Equilibrium Bubbles | Calculated |
| Annealed 1 hr at 1050°C | 500 | 2950 | 15,339 | 0.19 |
| 20% Cold Worked | 380 | 3400 | 14,146 | 0.24 |
| After 1 hr at | 450 | 3810 | 17,920 | 0.21 |
| 1050°C | 600 | 4150 | 10,355 | 0.40 |
| | 680 | 4240 | 15,284 | 0.28 |

irradiation temperatures they may have more void character. This conclusion is supported by the observation that grain boundaries are free of visible cavities at 550°C and below and decorated by large cavities at 600°C and above.

### 1.1.4 Conclusions

1. Large amounts of helium greatly increase the concentration of cavities during irradiation.

2. The cavities are probably near-equilibrium bubbles, but calculations indicate that the amount of helium present is less than that required to balance the surface tension restraint.

3. A cold-worked microstructure is stable for irradiation temperatures of 550°C and lower. It appears to be beneficial in reducing swelling.

4. Recovery and recrystallization are enhanced by irradiation at temperatures of 600°C and higher. Cold working offers no advantage in this temperature range.

5. Precipitation is greatly enhanced at all irradiation temperatures.

## 1.2 TEMPERATURE AND FLUENCE LIMITATIONS FOR A TYPE 316 STAINLESS STEEL CTR FIRST WALL - E. E. Bloom, F. W. Wiffen, and P. J. Maziasz

### 1.2.1 Purpose

Conventional iron-base alloys such as type 316 stainless steel are regarded as the most likely alloys for use as CTR first walls in at least the first generation fusion power reactors.[6,7] This choice is based on the extensive knowledge and experience with these alloys in gas, molten salt, and liquid metal coolants; well established fabricability and weldability; availability; and an extensive body of information on their response to neutron irradiation gained from the LMFBR programs.

At a neutronic wall loading of 1 MW/m$^2$ the first-wall flux of a fusion reactor is $3.7 \times 10^{14}$ n cm$^{-2}$ sec$^{-1}$, with about 20% of the neutrons with energies near 14 MeV. For a type 316 stainless steel first wall about 10 dpa (displacements per atom) and 200 at. ppm He will be produced per year of operation. This can be compared with about 60 dpa/year and 10 at. ppm/year neutronically generated helium in a mixed-oxide core LMFBR. It has been known for some time that a few atomic parts per million helium can markedly reduce the high-temperature tensile and creep-rupture ductility. This reduction of ductility coupled with fast-neutron-induced swelling and low-temperature hardening has led to predictions of first-wall lifetimes as short as two years.[6,8]

The purpose of this paper is to consider recently obtained results of irradiation experiments conducted in HFIR to obtain a more realistic assessment of temperature and fluence limitations on the lifetime of a type 316 stainless steel first wall than can be made solely on the basis of fast reactor irradiations. Initial criteria will be swelling and uniform strain as used by Kulcinski et al.[8] In HFIR, helium is produced by a two-step nuclear reaction with thermal neutrons: $^{58}Ni(n,\gamma)^{59}Ni$ followed by $^{59}Ni(n,\alpha)^{56}Fe$, and the high thermal and fast flux in HFIR

---

[6] B. Badger et al., *UWMAK-I, A Wisconsin Toroidal Fusion Reactor Design*, UWFDM-68, University of Wisconsin (November 1973).

[7] R. G. Mills, ed., *A Fusion Power Plant*, MATT-1050, Princeton University (August 1974).

[8] G. L. Kulcinski et al., "Radiation Damage Limitations in the Design of Wisconsin Tokamak Fusion Reactor," *Nucl. Technol.* 22: 20 (1974).

results in about 35 dpa and 1900 at. ppm He per year in stainless steel and thus better simulates the neutron response of a CTR first wall than does fast reactor irradiation. Samples of annealed and cold-worked type 316 stainless steel have been irradiated at 380 to 785°C over a range of damage levels up to about 60 dpa[9] and 4200 ppm He.[10] Swelling, tensile and creep-rupture properties, and microstructural changes have been reported previously.[11-13]

### 1.2.2 Evaluation of Data

In the range 380 to 600°C a cold-worked structure has superior swelling resistance over a solution-annealed structure. At about 60 dpa and 4200 at. ppm He a maximum density decrease of 3.3% occurred in the 20%-cold-worked structure, compared with 8.7% in the annealed structure. At the temperature for maximum swelling in fast reactor irradiation (550-600°C) the density decreases for both the cold-worked and the annealed alloys were significantly greater than for samples of the same heat irradiated in EBR-II under similar conditions.[14] This observation suggests that helium content, not dpa level, controls the swelling. Above 600°C the swelling of annealed and cold-worked structures is about the same because of recovery of the cold work, and the swelling increases with temperature instead of decreasing as in a fast reactor irradiation.

---

[9]Displacement per atom values are one-half of values previously reported. All dpa numbers in this contribution are consistent with the method of calculation recommended by the IAEA Specialists Meeting on Radiation Damage Units for Ferritic and Stainless Steels.

[10]Helium contents are revised from earlier published work, reflecting more complete measurements.

[11]F. W. Wiffen and E. E. Bloom, "Effect of High Helium Content on Stainless Steel Swelling," *Nucl. Technol.* 25: 113 (1975).

[12]E. E. Bloom and F. W. Wiffen, *The Effects of Large Concentrations of Helium on the Mechanical Properties of Neutron-Irradiated Stainless Steel*, ORNL-TM-4861 (May 1975); also to be published in *Journal of Nuclear Materials*.

[13]P. J. Maziasz, F. W. Wiffen, and E. E. Bloom, "Properties of Type 316 Stainless Steel Irradiated to Produce High Helium Contents and High Damage Levels," to be published in Proceedings of the International Conference on Radiation Effects and Tritium Technology for Fusion Reactors.

[14]P. S. Sklad and E. E. Bloom, ORNL unpublished results.

Swelling considerations thus limit wall temperature to about 600°C. Within this temperature limitation and the criterion of a maximum first-wall swelling of 10% at end of life,[6] the most pessimistic limitation that is set by our swelling results is a wall lifetime of greater than six years. Since this limit is based on a solution-annealed condition and correlation on the basis of dpa, less restrictive lifetimes can be predicted for cold-worked material and for correlation on the basis of helium content.

Tensile properties were altered in the same direction as for a fast-reactor irradiation but to a greater extent. Samples irradiated in the annealed condition to about 50 dpa and 3500 ppm He showed an increased yield strength between 350 and 600°C and, except at 350°C, a reduced ultimate tensile strength compared with the unirradiated condition. In the 20%-cold-worked condition yield and ultimate tensile strengths decreased at all irradiation temperatures. Both the annealed and cold-worked material exhibited little strain hardening following irradiation. Below 450°C the fracture strain is usually controlled by plastic instability, which is in turn related to the work hardening behavior. For annealed materials irradiation decreases the work hardening coefficient and thus the uniform strain. In type 304 stainless steel irradiated in the EBR-II this effect saturates at about 20 dpa at 0.5% uniform strain and 2.5% total elongation.[15] These values are consistent with type 316 stainless steel irradiated in HFIR to very high helium contents. Thus, we conclude that for temperatures below 450°C the behavior of stainless steel at high dpa and high helium contents is related primarily to hardening phenomena. The uniform strain will not drop below about 0.5% and should not be a limiting property.

With increasing temperature the effects of helium become more pronounced. At 500°C, 0.7% uniform strain was retained after 60 dpa and 4000 at. ppm He. At 575°C the uniform and total elongations drop below

---

[15]R. L. Fish et al., "Swelling and Tensile Property Evaluations of High-Fluence EBR-II Thimbles," p. 149 in *Effects of Radiation on Substructure and Mechanical Properties of Metals and Alloys*, *Am. Soc. Test. Mater. Spec. Tech. Publ.* 529, ed. by John Moteff, American Society for Testing and Materials, Philadelphia, 1973.

0.5% in the interval between 28 dpa, 1700 at. ppm He and 60 dpa, 4000 at. ppm He. At 650°C both the uniform and total elongations were zero for irradiations to about 60 dpa and 4200 ppm He. Using the criterion of 0.5% residual uniform elongation,[8] a first-wall temperature limit of 500 to 550°C would be imposed. Fluence limits are somewhat more difficult to judge because of synergistic effects between hardening and helium. However, if the 0.5% uniform strain criterion is used, 40 dpa at 550°C or 60 dpa at 500°C should be tolerable, allowing a minimum of four to six years CTR operation at a wall loading of 1 MW/m$^2$ (using again the pessimistic dpa correlation).

### 1.2.3 Summary and Recommendations

If swelling and uniform strain are used as performance criteria, 20%-cold-worked type 316 stainless steel apparently can be used as first-wall construction material with an expected lifetime of at least five years (50 dpa and 1000 at. ppm He) for design temperatures not exceeding 550°C. However, additional material behavior certainly should be considered. At 550°C thermal creep-rupture properties are drastically reduced (rupture life reduced by $5 \times 10^3$ as a result of irradiation to 40 dpa and 3000 ppm helium).[11] On the basis of tensile data a marked reduction in fatigue life is also expected and may limit the lifetimes of CTR devices operating in a pulsed mode. Radiation creep rates could also be limiting and have not yet been experimentally determined.

## 1.3 SWELLING AND MICROSTRUCTURAL CHANGES IN IRRADIATED VANADIUM ALLOYS — J. Bentley and F. W. Wiffen

### 1.3.1 Purpose

Vanadium-base alloys are potentially attractive for use as the first-wall structural material for fusion reactors because of (1) reasonably good strength, useful to about 800°C; (2) low activation rates compared with niobium or stainless steel, and thus much reduced problems with

after-heat and radioactive waste management;[16,17] and (3) a demonstrated resistance of vanadium-titanium alloys to irradiation-produced swelling and embrittlement.[18,19] Swelling and microstructural characterization have been completed on three vanadium alloys to further evaluate the effects of neutron irradiation and the potential for CTR use of these alloys.

### 1.3.2 Experiment Description

Specimens of V-10% Cr and VANSTAR-7 (V-9% Cr-3% Fe-1.3% Zr-0.05% C) with total interstitial impurity (C, N, O) contents of 770 and 1350 ppm (weight), respectively, have been irradiated in the form of tensile specimens in EBR-II at temperatures between 496 and 805°C to a neutron fluence of $1.5 \times 10^{22}$ n/cm$^2$ (>0.1 MeV), which corresponds to 17 dpa (calculated with the Lindhard model with 25-eV threshold). The measured helium content of an irradiated VANSTAR-7 specimen was 1.8 at. ppm.

### 1.3.3 Results

Swelling values were determined from immersion density measurements and from void distribution data obtained by transmission electron microscopy (TEM) and are shown in Table 1.3. The good agreement between the values of swelling calculated by the two methods is noteworthy. Quantitative data from the as-irradiated microstructure are also summarized in Table 1.3.

---

[16]D. Steiner and A. P. Fraas, "Preliminary Observations on the Radiological Implications of Fusion Power," *Nucl. Safety* 13: 353-62 (September-October 1972).

[17]D. Steiner, "Long-Lived Activities and Radioactive-Waste Management Associated with D-T Fusion Reactors," *Nucl. Fusion* 11: 307-08 (1971).

[18]F.W. Wiffen, "The Effect of Alloying and Purity on the Formatio and Ordering of Voids in BCC Metals," pp. 386-96 in *Radiation-Induced Voids in Metals*, ed. by J. W. Corbett and L. C. Ianniello, AEC Symp. Ser. 26, CONF-710601 (April 1972).

[19]R. Carlander, S. D. Harkness, and A. T. Santhanam, "Effects of Fast-Neutron Irradiation on Tensile Properties and Swelling Behavior of Vanadium Alloys," pp. 399-414 in *Effects of Radiation on Substructure and Mechanical Properties of Metals and Alloys, Am. Soc. Test. Mater. Spec. Tech. Publ.* 529, ed. by John Moteff, American Society for Testing and Materials, Philadelphia, 1973.

Table 1.3. Measured Swelling and Void Parameters for Two Vanadium-Base Alloys Irradiated in EBR-II[a]

| Irradiation Temperature (°C) | Immersion Density Change $-\Delta\rho/\rho$ (%) | Dislocation Density[b] ($cm^{-2}$) | Mean Void Diameter[c] (Å) | Total Void Concentration[b] ($cm^{-3}$) | Swelling (%) |
|---|---|---|---|---|---|
| | | V–10% Cr | | | |
| 496 | 0.08 | $2.6 \times 10^{10}$ | 80 | $1.1 \times 10^{14}$ | 0.003 |
| 580 | d | $2.4 \times 10^{10}$ | 93 | $1.4 \times 10^{14}$ | 0.006 |
| 690 | 0.91 | $8.1 \times 10^{9}$ | 1580 | $5.2 \times 10^{12}$ | 1.06 |
| 805 | d | $4.0 \times 10^{9}$ | 1690 | $5.3 \times 10^{12}$ | 1.35 |
| | | VANSTAR-7 | | | |
| 496 | 0.18 | e | 98 | $9.2 \times 10^{14}$ | 0.045 |
| 580 | d | e | 129 | $3.4 \times 10^{14}$ | 0.040 |
| 690 | −0.05 | $5.4 \times 10^{9}$ | ~1000 | $<10^{11}$ | ≈0 |
| 805 | d | e | ~1000 | $<10^{11}$ | ≈0 |

[a] Fluence $1.5 \times 10^{22}$ n/cm² (>0.1 MeV), 17 dpa (Lindhard Model), and 1.8 ppm He.

[b] Concentrations obtained from foil thicknesses measured by stereo microscopy.

[c] Diameter of the void of mean volume.

[d] Not determined.

[e] Not resolvable.

The microstructures of the V–10% Cr specimens irradiated at 496 and 580°C were similar, consisting of a dislocation network and some loops [see Fig. 1.12(a)] with a coarse distribution of small voids [see Fig. 1.12(b)], leading to negligible swelling. Also present was a fine distribution ($\approx 5 \times 10^{14}$/cm$^3$) of small unidentified precipitate particles (≈100 Å diam). The dislocation component of the V–10% Cr irradiated at 690 and 805°C was coarser [see Fig. 1.12(c)], and, although the void concentration was much less than at lower temperatures, the dramatic size increase resulted in appreciable swelling (≈1%). One interesting feature of the microstructure was the presence of a much higher dislocation density within about 1500 Å of the large voids [see Fig. 1.12(c)]. A comparison of the present results with data for irradiated vanadium[18,20] indicates that the addition of 10% Cr to vanadium, although significantly reducing the void concentration, does not necessarily reduce the swelling, as was previously found in a more limited study.[19]

Only in one sample of the VANSTAR-7 was the dislocation structure clearly resolved (690°C), and it consisted of a coarse network. In all other samples the dislocations were obscured by strongly diffracting regions distributed on a very fine scale. Diffraction patterns showed considerable diffuse scattering, often strongest along ⟨100⟩, and occasionally weak extra spots. Impurity pickup during irradiation may be responsible for the effect. At irradiation temperatures of 496 and 580°C the voids were larger and in greater concentration [see Fig. 1.12(d)] than in the V–10% Cr, but at irradiation temperatures of 690 and 805°C only occasionally were voids observed, often in association with precipitates that had been present in unirradiated specimens.

Limited TEM examination of V–20% Ti irradiated in EBR-II at temperatures between 370 and 805°C to fluences between 0.5 and $6.1 \times 10^{22}$ n/cm$^2$ (>0.1 MeV) has failed to reveal the presence of voids, the only damage structure observed being a dislocation network. This result is in agreement with previous observations[18,19] and new work (Sect. 1.4).

---

[20] J. D. Elen, G. Hamburg, and A. Mastenbroek, "Voids in Vanadium, Niobium, and Molybdenum by Fast Neutron Irradiation at High Temperatures," *J. Nucl. Mater.* 39:194 (1971).

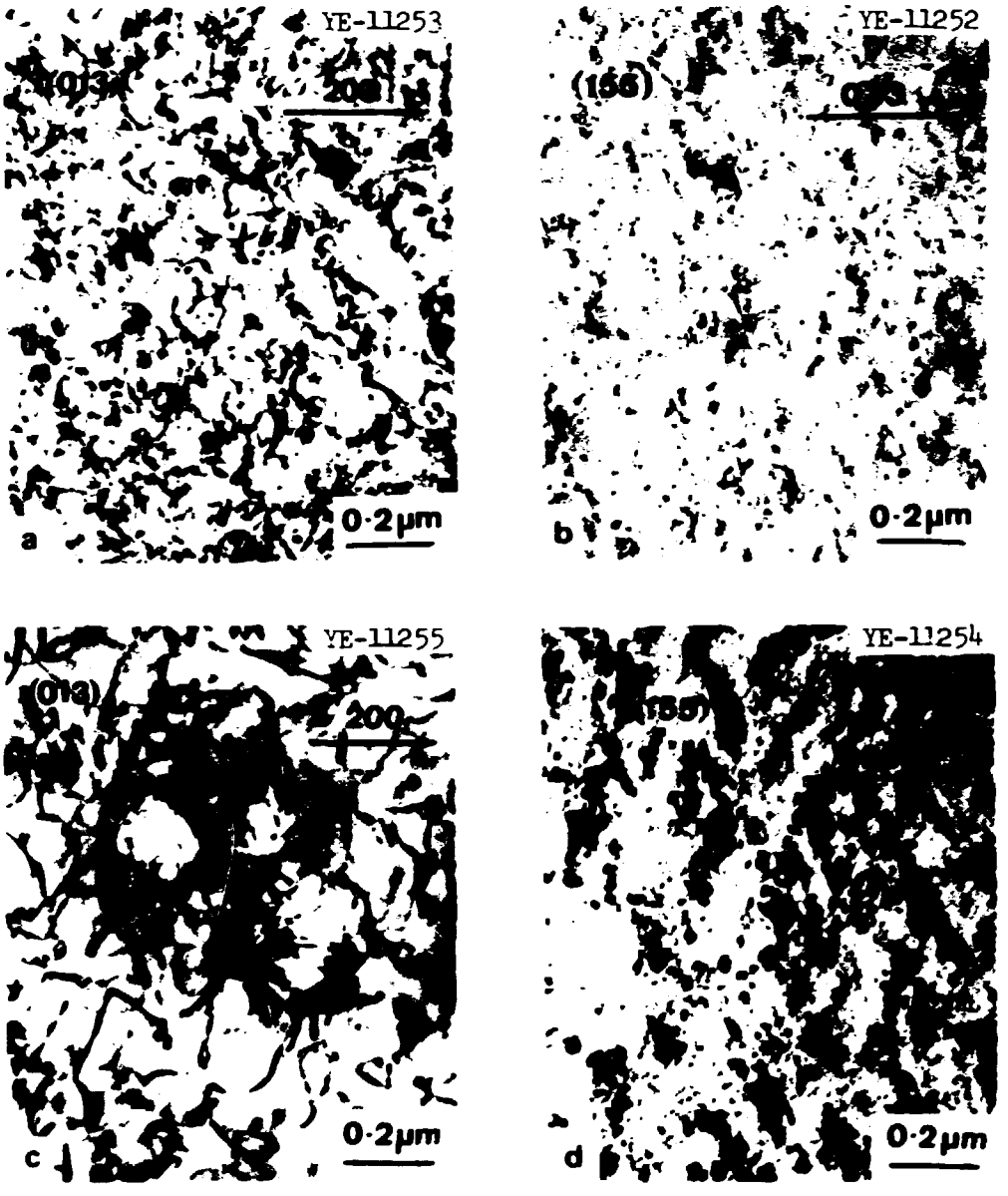


Fig. 1.12. Electron Micrographs Showing Damage Structures in Vanadium Alloys Irradiated to a Fluence of $1.5 \times 10^{22}$ (>0.1 MeV). Diffraction vectors and beam directions as indicated. (a) V–10% Cr, irradiated at 496°C. (b) V–10% Cr, irradiated at 580°C. (c) V–10% Cr, irradiated at 805°C. (d) VANSTAR-7, irradiated at 580°C.

### 1.3.4 Conclusions

This work has confirmed the resistance to swelling of neutron-irradiated V–20% Ti and shown that V–10% Cr and VANSTAR-7 do not have an intrinsic swelling resistance. The results show that vanadium alloys as a class cannot be regarded as swelling resistant. For CTR application, a comprehensive study of swelling would be a required part of the radiation effects evaluation within any vanadium alloy development program.

## 1.4 MECHANICAL PROPERTIES OF IRRADIATED V–20 wt % Ti — J. A. Horak and F. W. Wiffen

### 1.4.1 Purpose

The purpose of this work is to determine the postirradiation tensile and creep properties of V–20 wt % Ti.

### 1.4.2 Experiment Description

Tensile samples of V–20 wt % Ti that had been annealed for 1 hr at 900°C before irradiation were irradiated in EBR-II to fluences between 0.5 and 6.1 × $10^{22}$ n/cm$^2$ (>0.1 MeV) at temperatures between 370 and 900°C, respectively. After irradiation the tensile samples were measured for swelling and examined with x-ray diffraction for absorption of interstitials. Samples were then cut for transmission electron microscopy, and the material was tested under tensile and creep conditions at temperatures up to 800°C.

### 1.4.3 Results

The results obtained to date showed essentially little or no swelling of these alloys after this irradiation temperature history in EBR-II. Preliminary measurements revealed no changes in the mechanical properties that would be detrimental to the use of V–20 wt % Ti as the first wall of a fusion reactor.

### 1.4.4 Discussion

The mechanical properties obtained to date are preliminary and require a detailed evaluation of the stress-strain curves and the values

obtained from them before a complete evaluation is possible. This will be conducted in the next few months and will give us a quantitative assessment of the mechanical behavior of the irradiated V–20% Ti alloys.

### 1.4.5 Conclusions

After an irradiation of up to $6 \times 10^{22}$ n/cm$^2$ (>0.1 MeV) at irradiation temperatures from 400 to 900°C we observed essentially no swelling and little loss of ductility in the V–20 wt % Ti tested.

## 1.5 RADIATION DAMAGE CALCULATIONS — T. A. Gabriel,[21] J. D. Amburgey,[21] and N. M. Greene,[21]

### 1.5.1 Purpose

The neutron spectra that are expected in a controlled thermonuclear reactor (CTR), especially near or at the first wall, will be considerably different in shape and magnitude from those that are presently available from fission reactors, from 14-MeV neutron sources, or from other types of irradiation facilities. Because of the higher average neutron energy anticipated in the CTR environment, greater gas production by direct reactions, as well as higher average recoil energies, can be anticipated. Since CTR-type neutron spectra are not presently available for experimental measurements, one needs a calculational method by which radiation-damage effects in structural materials (i.e., gas production and nuclear displacements) can be simulated, studied, evaluated, and correlated in different neutron environments.

### 1.5.2 Procedure

A heavy charged-particle recoil data base has been obtained for neutrons with energies of up to 20 MeV and for most of the elements of interest to the CTR community. The elements included in the data base are Al, Ti, V, Cr, Mn, Fe, Co, Ni, Cu, Zr, Nb, Mo, Ta, W, Pb, Mg, Be, C, Au, Si, B, N, and Li. The inclusion of such elements as nitrogen, boron, and lithium is due to their relatively large gas-production cross sections

---

[21] Neutron Physics Division.

and to the fact that these elements are usually found as impurities in most structural materials.

All neutron reactions, including elastic, inelastic, $(n,2n)$, $(n,3n)$, $(n,p)$, $(n,n\alpha)$, and $(n,\gamma)$, that have cross sections available from ENDF/B-IV have been processed and placed in the data base. For elastic, inelastic, $(n,2n)$, $(n,n'p)$, $(n,n'\alpha)$, and $(n,3n)$ reactions, a modified version of the XLACS module from the AMPX code system[22] was used to calculate the heavy-charged-particle recoil spectra. For elastic and inelastic resolved reactions where angular distributions are usually available, these distributions were used in obtaining the heavy recoil spectra. For reactions such as $(n,2n)$, $(n,n'p)$, etc., where only the secondary-neutron-energy spectra are available, several simplifying assumptions (such as the one-neutron emission model and isotropic emission in the center-of-mass system) were used to obtain the recoil spectra. For neutron absorption reactions such as $(n,p)$, $(n,\alpha)$, etc., the methods of Jenkins,[23] Doran,[24] and Parkin[25] were used with one modification: an effective Coulomb barrier was used as the lower energy by which a charged particle can be emitted. For $(n,\gamma)$ reactions, a Monte Carlo program was written. The secondary gamma-ray energies were obtained from the nuclear data sheets.

Some analysis using a Monte Carlo program was carried out to check the validity of the one-neutron emission model. For the $(n,2n)$ reaction, the charged-particle recoil spectra are not greatly modified by the emission of the second neutron. The other multiemission reactions have not been studied in enough detail to derive any general conclusions.

---

[22]N. M. Greene et al., *AMPX: A Modular Code System for Generating Coupled Multigroup Neutron-Gamma Libraries from ENDF/B*, ORNL-TM-3706 (in press).

[23]J. D. Jenkins, "Primary-Recoil Atom Spectra from ENDF/B Data," *Nucl. Sci. Eng.* 41: 155–63 (1970).

[24]D. G. Doran, "Neutron Displacement Cross Sections for Stainless Steel and Tantalum Based on a Lindhard Model," *Nucl. Sci. Eng.* 49: 130–44 (1972).

[25]D. M. Parkin and A. N. Goland, *A Computational Method for the Evaluation of Radiation Effects Produced by CTR-Related Neutron Spectra*, BNL-50434 (September 1974).

An analysis program that uses the calculated results in the data base has also been written. This code calculates (1) displacement cross sections and damage energy cross sections for single elements or alloys using the Lindhard theory,[26,27] (2) spectral averaged cross sections for production of displacements, damage, and gas (p, D, T, $^3$He, α), and (3) spectral averaged primary recoil spectra. Examples of some calculated results can be seen in Figs. 1.13 and 1.14. Figure 1.13 shows the total displacement cross section for copper as a function of neutron energy.

---

[26] J. Lindhard et al., "Range Concepts and Heavy Ion Ranges (Notes on Atomic Collisions II)," *Mat. Fys. Medd. Dan. Vid. Selsk.* 33: 1–42 (1963).

[27] M. T. Robinson and I. M. Torrens, "Computer Simulation of Atomic-Displacement Cascades in Solids and the Binary-Collision Approximation," *Phys. Rev. B* 9(12): 5008–24 (1974).

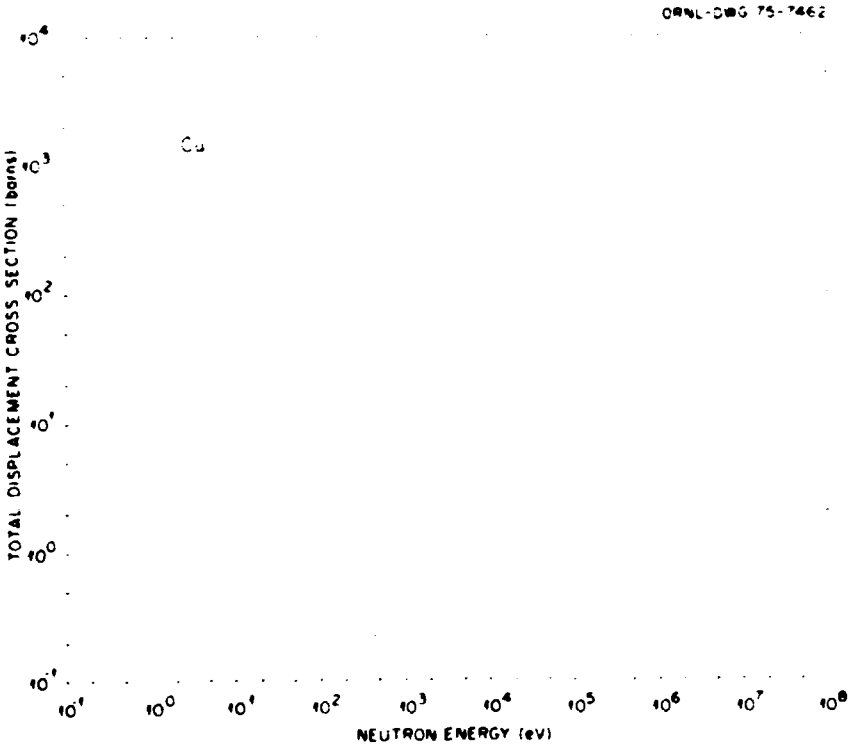


Fig. 1.13. The Total Displacement Cross Sections for Copper as a Function of Neutron Energy.

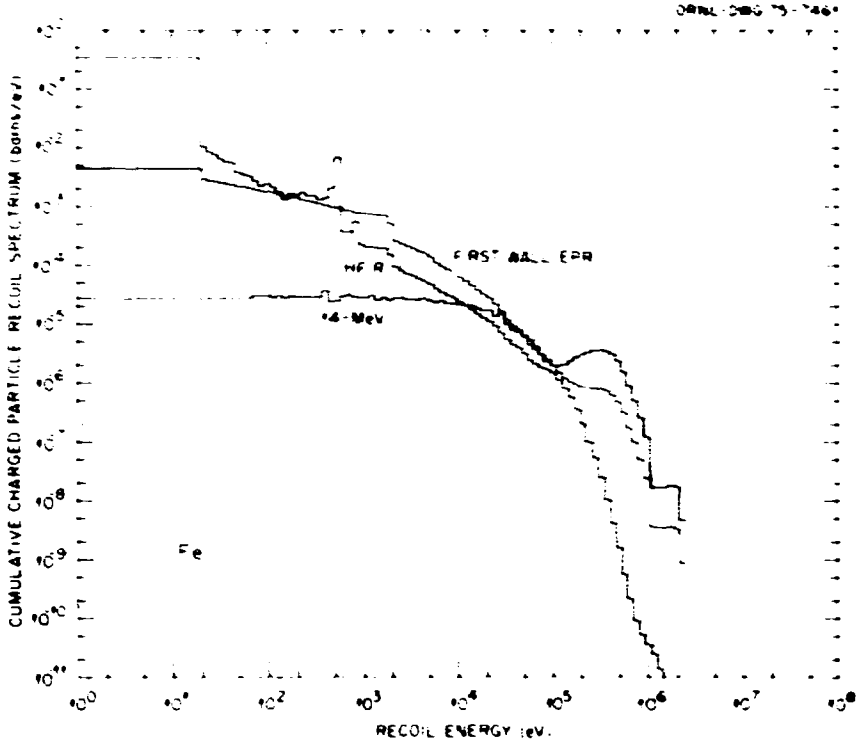


**Fig. 1.14. Calculated Heavy Charged-Particle Recoil Spectra in Iron Expected in Three Different Neutron Environments.**

Figure 1.14 shows the expected averaged heavy charged-particle recoil spectra in iron for a 14-MeV neutron spectrum, a first-wall experimental power reactor neutron spectrum, and a HFIR neutron spectrum. The peaks at approximately 600 eV on the HFIR recoil spectrum are due primarily to thermal neutron capture in iron.

A report describing the calculational methods and results will be published later. The results will include displacement and damage energy cross sections for all the elements in the data base, as well as for several alloys of interest, gas-production cross sections for several elements and alloys, and spectral-averaged primary knocked-on atom.

## 1.6 EVALUATION OF IRRADIATION FACILITIES FOR CTR MATERIALS DEVELOPMENT — J. A. Horak

### 1.6.1 Purpose

This work is directed toward evaluating existing and proposed neutron irradiation facilities for use in CTR materials development. One aspect is to identify those material properties and experimental parameters that are most important to materials performance in the fusion radiation environment. After the most important properties and parameters are identified the evaluation is to identify the irradiation facilities that are needed for testing materials under as close to CTR conditions as is feasible and/or reasonably achievable from economic, time, and manpower criteria.

### 1.6.2 Criteria

1. *Experimental Volume.* Because of the large number of properties that must be measured and the large number of materials and materials variables that need to be considered, experimental volumes of hundreds of cubic centimeters are required to conduct comprehensive irradiation programs. For example, tensile, creep, fatigue, and swelling behavior must be determined over the range of temperature and stress conditions expected in fusion reactor service for the materials and the metallurgical states that have been proposed.

2. *Damage Rate.* The facilities used for testing engineering properties must be capable of providing damage rates at least equal to those expected in eventual fusion reactors. Rates accelerated by a factor five or more would be desirable for evaluating radiation effects in components expected to have 10 to 20-year lifetimes. This will require 14-MeV neutron sources having fluxes of the order of those expected in fusion reactors or fission reactors having fluxes exceeding $5 \times 10^{14}$ n $cm^{-2}$ $sec^{-1}$ (>0.1 MeV) and average energy of about 0.8 MeV.

3. *Temperature and Stress Measurement and Control.* The damage produced at elevated temperatures is extremely sensitive to irradiation temperature and probably to stress state. In-reactor deformation also depends critically on these variables. Any quantitative assessment of

radiation effects requires the ability to measure and control temperature during irradiation.

4. *Duplication of the Fusion Reactor's Neutron Environment.* The damage produced in a material is sensitive to the energy spectrum of the neutrons producing the damage. Neutron energy affects not only the amount and distribution of displaced atoms but also the probability of production of transmutation products, some of which influence the amount and the final form of the damage.

### 1.6.3 Evaluation of Existing Sources

Experimental parameters for existing radiation facilities are listed in Table 1.4 along with an evaluation of their possible uses. None of the facilities satisfies all the criteria listed above, so some compromise is necessary in developing a fusion reactor radiation effects program for the next decade or so.

While the Rotating Target Neutron Source can supply the necessary high-energy neutron component, it falls far short of the flux and experimental volume requirements. Its use will likely be confined to low-fluence experiments aimed at correlating fission and fusion reactor neutron damage.

Fission reactors can meet all the criteria given above except for providing a flux of 14-MeV neutrons. Consequently they do not duplicate the fusion reactor environment, but under certain conditions they can provide a good simulation of it. High-energy neutrons produce larger displacement cascades than do lower energy neutrons, but there is no experimental evidence that this causes any qualitative change in the form of the final damage. The quantitative differences that have been found are in general agreement with theoretical predictions. For example, Merkle[28] showed that the large cascades created by 14-MeV neutrons were actually composed of several small cascades that produced damage (vacancy loops) identical to that produced by lower energy neutrons. Borg and Dienes[29] and Damask et al.[30] used short-range order to measure the effect of neutrons of different energy in producing damage and found differences

---

[28]K. L. Merkle, *Nucl. Technol.* 22: 66 (1974).

[29]R. J. Borg and G. L. Dienes, *J. Appl. Phys.* 46: 99 (1975).

[30]A. C. Damask et al., *Trans. Am. Nucl Soc.* 21: 166 (1975).

## Table 1.4. Irradiation Facilities for CTR Bulk Radiation Effects Studies

| Facility | Flux Above 0.1 MeV (n $cm^{-2}$ $sec^{-1}$) | Experimental Volume at This Flux ($cm^3$) | Maximum Number of Positions[a] | Instrumented Control[b] | Suggested Use |
|---|---|---|---|---|---|
| **Experimental Breeder Reactor-II** | | | | | |
| Row 2 | $20.7 \times 10^{14}$ | 220 | 3 | No[c] | Screening engineering materials at high dpa. |
| Row 4 | 18.1 | 220 | 5 | No[c] | |
| Row 5 | | 220 | 4 | T, σ | |
| Row 7 | 9.6 | 220 | 7 | No[c] | |
| Row 8 | 7.5 | 220 | 12 | No[c] | |
| **High Flux Isotope Reactor** | | | | | |
| Peripheral Target Positions[d] | 14.8 | 10 | 6[d] | No[c] | High helium and dpa in alloys containing nickel. |
| **Removable Beryllium Reflector Positions** | | | | | |
| Large | 5.3 | 30 | 4 | T, σ | Quantitative Measurements of T and σ effect effects in alloys containing nickel. |
| Small | 6.4 | 10 | 4 | T, σ, $\phi_t/\phi_f$ | |
| **Oak Ridge Research Reactor (Core Positions)** | | | | | |
| C-3 | 4 | 720 | 3 | T,σ, $\phi_t/\phi_f$ environment | Highly quantitative data, especially in alloys containing nickel. |
| E-3 | 3 | 720 | 3 | T,σ,$\phi_t$,$\phi_f$ environment | |
| Rotating Target Neutron Source | 0.005 (14 MeV) | 3 | 1 | T,σ, environment | Correlation experiments fundamental studies. |

[a] Number existing in reactor, not the number available for the CTR program.

[b] T = irradiation temperature, σ = stress, $\phi_t$ = thermal neutron flux, and $\phi_f$ = fast neutron flux.

[c] Can achieve passive temperature control with heat pipes and, thereby stress control of pressurized tubes in heat pipes.

[d] Thirty similar high-flux positions available in target rod positions.

that were in quantitative agreement with theoretical predictions. We conclude that fission reactors do an adequate job of simulating the displacement component of damage introduced by 14-MeV neutrons. The problem with their use lies in matching the formation of transmutation products. Of these the most critical is helium. For materials containing nickel appropriate amounts of helium can be generated by the two-step reaction with thermal neutrons according to the sequence:

$$^{58}Ni(n,\gamma)^{59}Ni \qquad \alpha = 4.2 \text{ b}$$
$$^{59}Ni(n,\alpha)^{56}Fe \qquad \alpha = 7.2 \text{ b}$$

(note: $1 \text{ b} = 10^{-28}\text{m}^2$).

Through the proper control of the thermal-to-fast neutron ratio, the proper mixture of displacements and helium atoms can be provided in materials containing nickel. We conclude that although fission reactors do not duplicate the fusion reactor spectrum, they provide an adequate simulation of its most important effects.

The evaluation indicates that because of its large experimental volume EBR-II would best be used for the screening of large numbers of engineering alloys at high fluences. The best use of the HFIR peripheral target positions (PTP) would be for screening studies for alloys that contain nickel since relevant helium concentrations could be produced by the high thermal neutron flux in this reactor. The removable beryllium (RB) positions in HFIR can be utilized for instrumented testing where temperature and stress are controlled to provide more quantitative information on the materials than can be obtained in the uninstrumented PTP positions.

Of the existing fission neutron irradiation facilities the C3 and E3 positions of the Oak Ridge Research Reactor, ORR, provide the best combination of fast neutron flux, experimental volume, and ability to control temperature, stress, and chemical environment during irradiation. Because of the long fuel elements used in ORR (31 in. or 0.79 m) several ratios of thermal to fast flux can be attained in one experiment; this will result in several different He/dpa ratios in one instrumented-controlled irradiation assembly. We recommend that these positions in the ORR and the HFIR-RB positions be utilized to determine the highly quantitative data that are required for the design of CTR structural components.

Table 1.5 summarizes information on proposed high-energy neutron irradiation sources. Of these sources the one that seems to have the most potential for CTR materials development is the $D^+$-lithium source. For a 100-mA beam of 40-MeV $D^+$ on lithium a neutron flux of $3 \times 10^{14}$ n $cm^{-2}$ $sec^{-1}$ of about 14-MeV neutrons would be available in experimental volume of 80 $cm^3$, and the volume available for a flux of $1 \times 10^{14}$ n $cm^{-2}$ $sec^{-1}$ is about 400 $cm^3$. This is the largest combination of experimental volume and high flux available of any of the proposed neutron facilities. This is the only source that will enable one to get hundreds of samples to the required fluence of $10^{22}$ n/$cm^2$ in reasonable testing times.

### 1.6.4 Conclusions

Our conclusions are that the Oak Ridge Research Reactor is an easily instrumented and controlled facility and may be useful for developing CTR structural materials, especially for those alloys that contain nickel. EBR-II should be used for screening alloys that are potential candidates at the high fluences obtainable in this reactor in about one year of operating time. The PTP positions of HFIR would be best used to produce

Table 1.5. Irradiation Conditions for Proposed Fusion Neutron Irradiation Sources

| Irradiation Source | Neutron Flux (n $cm^{-2}$ $sec^{-1}$) | Experimental Volume at this Flux ($cm^3$) |
|---|---|---|
| Upgraded RTNS | $0.1 \times 10^{14}$ (14 MeV) | ≈3[a] |
| Gas target | 2 | 20[b] |
| D-Be | 0.02 | 3[c] |
| D-Li | 3 (>10 MeV) | 100[c] |

[a] J. C. Davis, LLL, presentation at Argonne Conference on Neutron Sources for CTR Materials and Surface Studies, July 16, 1975.

[b] C. R. Emigh, LASL, presentation at Argonne Conference on Neutron Sources for CTR Materials and Surface Studies, July 16, 1975.

[c] M. J. Saltmarsh, ORNL, presentation at Argonne Conference on Neutron Sources for CTR Materials and Surface Studies, July 16, 1975.

high helium concentrations and dpa in alloys containing nickel. The RB positions, in which some instrumented control is possible, should be used to obtain more quantitative data than can be obtained in the PTP positions. Of the neutron sources that have been proposed to be built in the next ten years, we conclude that the $D^+$-lithium source offers the best combination of experimental volume and neutron flux for CTR materials development.

## 1.7 STATUS OF REACTOR IRRADIATIONS

### 1.7.1 HFIR Irradiation of Nickel-Base Alloys — F. W. Wiffen

#### 1.7.1.1 Purpose

Nickel alloys are one of several classes of material of potential interest for use as structural materials in CTRs. Of the conventional alloys available without need for extensive development, this is the only class that provides an alternative to the austenitic stainless steels. Nickel alloys have been specified in one reactor conceptual design,[31] mainly on the basis of potentially greater resistance to neutron radiation damage than is found in the austenitic stainless steels.

Irradiation of alloys containing nickel in the HFIR produces helium through the two-step thermal neutron capture sequence

$$^{58}\mathrm{Ni}(n,\gamma)^{59}\mathrm{Ni}\ ,$$

$$^{59}\mathrm{Ni}(n,\alpha)^{56}\mathrm{Fe}\ .$$

At the same time, the fast-neutron component of the HFIR spectrum produces displacement damage, and thus the two main components of CTR spectrum radiation damage are simulated.

Two alloys have been selected as representative of the whole class of nickel-base alloys. Inconel 600 has been included as a representative of those alloys strengthened only by solid-solution alloy additions;

---

[31] R. G. Mills, ed. *A Fusion Power Plant*, MATT-1050, Princeton University (August 1974).

Nimonic PE-16 has been included as representative of those more complex nickel alloys strengthened by both solid-solution and precipitation hardening.

Irradiation of these two alloys in the PTP of the HFIR flux-trap region can be used to simulate CTR operating fluences and design temperatures. Evaluation of irradiated samples will help determine the expected swelling, mechanical properties, and microstructural response if these alloys are specified for CTR structural components.

1.7.1.2 Experiment Description

Experiments HFIR-CTR-3, -5, and -6 each contained 11 rod tensile specimens 39 mm in length with a reduced gage section 2 mm in diameter and 18 mm long. Irradiation temperatures ranged from 300 to 700°C and were attained by a helium-filled gap, which provided resistance to the radial flow of the nuclear heat produced in the specimen to the specimen holder operating near reactor ambient temperature (≈55°C). The desired temperature is thus set by adjusting the gas gap for the heat produced by the known heating rate at each specimen location.

1.7.1.3 Experiment Status

Irradiation of HFIR-CTR-3, -5, and -6 has been completed. Each was in the reactor for approximately 92 days at full power, for reactor midplane fluences of about $1.2 \times 10^{22}$ n/cm$^2$ (>0.1 MeV). Damage levels at the midplane are about 8 dpa and helium levels 1000 at. ppm in PE-16 samples and 1800 at. ppm in Inconel 600 samples. Damage calculated for specimens near the ends of the capsules is 30 to 40% of the midplane values.

The irradiation capsules have been disassembled and the samples recovered. Immersion density measurements are now under way. Further evaluation will include tensile tests, transmission electron microscopy, and metallography.

Similar experiments with the goal of higher fluences, to simulate longer CTR operation, are planned, and engineering design is near completion.

### 1.7.2 HFIR Irradiations of SAP to Produce High Helium Contents — P. J. Maziasz and K. Farrell

#### 1.7.2.1 Purpose

It has been proposed that SAP (Sintered Aluminum Product) may be a good candidate for use as the first-wall material of a CTR (Controlled Thermonuclear Reactor). To examine the feasibility of this proposal, tests are now under way to determine the effects of gas contents expected during CTR first-wall operation on the mechanical properties of SAP.

HFIR irradiation of samples doped with $^{6}Li$ has been chosen to simulate CTR irradiation of SAP. During irradiation, displacement damage is produced by the fast-neutron component of the HFIR spectrum and gas production (both tritium and helium) result from the thermal neutron reaction:

$$^{6}Li + n \rightarrow {}^{4}He + {}^{3}H \ .$$

The reaction cross section is about 950 b ($9.5 \times 10^{-26}$ m$^2$) for thermal neutrons.

#### 1.7.2.2 Experiment Description

Sintered Aluminum Product samples doped with 96%-enriched $^{6}Li$ have been prepared to our specification. Compositions of the four batches are given in Table 1.6. The $Al_2O_3$ content, near 20%, is higher than the intended 10.5%. However, the amount is secondary in importance to the way in which the oxide particles are dispersed.

Table 1.6. Chemical Composition of Lithium-Doped SAP

| Batch | $Al_2O_3$ (%) | Lithium (wt ppm) |
|---|---|---|
| 1 | 20.0 | <1 |
| 2 | 17.3 | 1.4 |
| 3 | 17.7 | 45 |
| 4 | 24.5 | 174 |

We irradiated 36 samples in a three-tube irradiation experiment in one of the PTP sites of the HFIR. In this experiment the rod tensile samples were in contact with the reactor coolant water during irradiation, at 55°C. Before assembly of the experiment, immersion density measurements were made on each of the specimens for irradiation.

1.7.2.3 Experiment Status

The experiment was irradiated in HFIR during cycles 118b and 120, for 3858 MWD of reactor power. The equivalent operating time at full power is 925.83 hr and resulted in the fluence on the experiment of 1.4 to 4.6 × $10^{21}$ n/cm$^2$ (>0.1 MeV). The $^6$Li burnup was calculated to be 94 to 99+%.

The experiment has been disassembled; the samples have all been recovered and cleaned and are now being measured for postirradiation density change. Future plans include as-irradiated mechanical properties determination and mechanical properties measurements after annealing to temperatures in the 350 to 450°C range to produce gas coalescence. Further experiments will be undertaken, pending results obtained from the tests at 350 to 450°C.

Tensile properties measured on the unirradiated control samples are given in Table 1.7. There was no significant variation in the mechanical properties between the four batches of material.

Table 1.7. Engineering Mechanical Properties of Unirradiated SAP as a Function of Temperature from 20 to 500°C

| Temperature (°C) | 0.2% Offset Yield Stress | | Ultimate Tensile | | Elongation, % | | Reduction of Area (%) |
|---|---|---|---|---|---|---|---|
| | (psi) | (MPa) | (psi) | (MPa) | Uniform | Total | |
| 200 | 55,800 | 375 | 67,500 | 405 | 2.82 | 4.14 | 8.28 |
| 300 | 29,300 | 202 | 31,300 | 216 | 0.30 | 0.34 | 1.35 |
| 400 | 22,100 | 152 | 22,500 | 155 | 0.35 | 0.35 | 0.91 |
| 500 | 15,900 | 110 | 16,000 | 110 | 0.25 | 0.25 | 2.2 |

### 1.7.3 Helium Implantation in Potential CTR Structural Materials — J. A. Horak

#### 1.7.3.1 Purpose

This experiment is designed to produce a homogeneous helium distribution in potential CTR structural materials, with helium contents equivalent to that anticipated in a CTR first wall after a reasonable lifetime. A major portion of the experiment is to inject the alloys with helium from the cyclotron and then to irradiate in EBR-II to produce a known helium per dpa level. Identical samples will be irradiated in HFIR and/or ORR to produce the helium and displacement damage simultaneously. After the two types of irradiations the dimensional and mechanical properties obtained by the two different methods of producing helium and displacement damage will be compared in an attempt to correlate the two different methods of producing helium and displacement damage in potential CTR structural materials. The degree of correlation achieved will determine the extent to which the method of gas implantation followed by neutron irradiation can be utilized for the development of materials for CTRs.

#### 1.7.3.2 Experiment Description

The experiment consists of injecting helium with the Oak Ridge Isochronous Cyclotron, ORIC, into solution-annealed type 316 stainless steel, the same alloy solution annealed and then 20% cold worked, V–20% Ti, V–15% Cr–5% Ti, and PE-16 in various thermodynamic states. The samples are placed in a holder in which rapidly moving cold water (≈20°C) is in contact with a sheet of the desired sample material and a second group of mechanical properties samples is placed over the interstices of the aforementioned sheet. The sample holder is moved back and forth in front of the alpha beam, which has previously gone through an energy degrader to produce a uniform helium concentration through the thickness of the mechanical properties samples. All components of the present facility for injecting helium into sheet material are water cooled to enable us to utilize all the beam current that exists at ORIC.

### 1.7.3.3 Results

We have successfully injected helium into material to produce 300 tensile specimens for subsequent irradiation in EBR-II and for testing without the irradiation. We have achieved helium concentrations of 70, 90, and 200 at. ppm. Table 1.8 gives the materials, number of samples, and the helium levels implanted. During the injection of helium into the sheet material we were able to operate the cyclotron at 21 μA of electrical beam current. This produced a 5-μA alpha particle current into the samples. This is a factor of 5 greater rate of helium deposition than had been achieved in previous injections into alloys at the ORIC and was achieved without appreciably increased sample heating.

Table 1.8. Helium Concentrations Implanted in Potential CTR Structural Alloys

| Material | Condition[a] | Number of Samples for Each Helium Content in at. ppm | | |
|---|---|---|---|---|
| | | 70 | 90 | 200 |
| Type 316 Stainless Steel | Solution annealed | 10 | 25 | |
| Type 316 Stainless Steel | 20% Cold worked | | 26 | 13 |
| V–20% Ti | Solution annealed | | 37 | 37 |
| V–15% Cr–5% Ti | Solution annealed | 37 | 37 | |
| Nimonic PE-16 | Solution annealed | 6 | 25 | |
| Nimonic PE-16 | Aged | 20 | | 25 |

[a]Solution anneal precedes other treatments.

### 1.7.3.4 Discussion

The helium levels attained are relevant to projected early CTR operations. Approximately 60 at. ppm of helium is the anticipated end-of-life concentration in type 316 stainless steel for fusion Experimental Power Reactor (EPR), and we have achieved that helium level in the stainless steel. In addition, the 200 ppm of helium in the type 316 stainless steel represents one full year of operation of a CTR at a wall loading of 1 $MW/m^2$, which is the projected wall loading of early CTRs.

We have produced helium levels in the vanadium alloys associated with one, two, and four years of first-wall lifetime at a wall loading of 1 $MW/m^2$.

### 1.7.4 EBR-II Row 8 Experiment — F. W. Wiffen, J. Bentley, J. A. Horak, and J. W. Woods

#### 1.7.4.1 Purpose

The goals of this experiment are to determine the effects of neutron irradiation on materials of interest for possible CTR application under conditions of known and controlled irradiation temperature. Samples that have been included in the experiment will investigate the effect of alloying on swelling and microstructural response to neutron irradiation of bcc refractory alloys and will define the effect of helium injected before reactor irradiation on the postirradiation mechanical properties and swelling.

#### 1.7.4.2 Experiment Description

This is a two-pin experiment developed by LASL for irradiation in Row 8 of EBR-II. The prime goal of the LASL experimenters is to explore the response of samples of ceramic insulators to neutron irradiation at accurately known irradiation temperatures. ORNL has included metal samples of interest to the CTR program through the courtesy of the LASL experimenters.

The two pins in this experiment are standard capsules for a B-7A subassembly. Each of the pins contains a heat pipe, one to operate at 600°C and the other at 800°C. Flat coupon-type samples are accommodated between the heat pipe and the containment tube. Nuclear-heated, sodium-filled subcapsules with temperatures controlled by the gas gap to the containment tube are located below each of the heat pipes. These are designed to operate at 500 and 700°C.

Samples to determine the effect of alloying on swelling in the bcc refractory metals have been included at each of the four irradiation temperatures. All materials were given a recrystallization anneal.

The materials included are listed below:

Niobium alloys: Nb, Nb–1% Zr;

Vanadium alloys: V, V–1% Ti, V–1.3% Zr;

Molybdenum alloys: Mo, Mo–0.5% Ti, Mo–1% Cr, TZM (Mo–0.5% Ti–0.08% Zr).

Samples that have been included to determine the effect of preirradiation injected helium on postirradiation properties include Nb, Nb–1% Zr, Mo, V–20% Ti, V–15% Cr–5% Ti, Nimonic PE-16, and type 316 stainless steel. Both helium-free and helium-injected samples have been included, and details of the helium injection are given in Sect. 1.7.3 of this report. The Nb, Nb–1% Zr, and Mo samples were injected previously.[32]

#### 1.7.4.3 Experiment Status

Specimens have been prepared and encapsulated at ORNL and are being shipped to LASL for inclusion in the assembly of the experiment and transfer to EBR-II for irradiation.

### 1.7.5 EBR-II Row 7 Experiment — E. E. Bloom

#### 1.7.5.1 Purpose

This irradiation is a joint experiment between programs at ORNL sponsored by ERDA Divisions of Reactor Research and Development, Controlled Thermonuclear Research, and Physical Research. The objectives of the experiment are to (1) determine the in-reactor fracture strain of 20%-cold-worked type 316 stainless steel, (2) determine the effects of preirradiation microstructure on the mechanical properties of low-swelling solid-solution alloys, (3) investigate the effects of pre-injected helium and irradiation temperature on bulk irradiation damage to candidate CTR first-wall materials, and (4) conduct a series of experiments designed to provide information on the mechanisms of irradiation creep, solute precipitation, and segregation during irradiation and fracture mechanisms in irradiated materials.

---

[32] F. W. Wiffen, *Fusion Technology Studies Progress Report for Period Ending Dec. 31, 1972*, ORNL-TM-4156 (May 1973), pp. 1–12.

### 1.7.5.2 Experiment Description

To attain temperatures above the EBR-II sodium coolant temperatures, samples will be contained in subcapsules that are heated by gamma heating and in which temperature control is achieved either by gas gaps or by heat pipes. The feasibility of the gas gap capsules has been demonstrated in several EBR-II experiments (e.g., X034, X035, X100, X100A). Heat pipes, designed by LASL personnel, are presently used by several EBR-II experiments (LASL, NRL, and HEDL) and, thus, feasibility of their use has been demonstrated. The heat pipes to be used in this experiment will be designed and built in cooperation with LASL personnel.

### 1.7.5.3 Experiment Status

Final specimen layout for this experiment is under way, and engineering design, including heat transfer calculations, is about 30% completed. Specimen preparation is under way, and the goal date for completion of the experiment assembly is May 15, 1976.

## 2. SURFACE STUDIES

R. E. Clausing

L. C. Emerson J. C. Twichell[1] R. J. Colchin[1] L. Heatherly

One of the major problems in fusion reactor technology is that of plasma contamination by nonhydrogenic materials released from the first wall of the fusion device. Such contamination is particularly detrimental in present-day torroidal devices, such as the Oak Ridge Tokamak (ORMAK). Small fractions of high-Z ions in the plasma of Tokamak fusion devices will greatly increase ignition temperatures and energy losses from the plasma.[2]

An experimental study has been initiated to assist in the identification and control of the impurities emanating from the first wall in ORMAK. The initial phases of the study have been concerned with the analysis of ORMAK wall materials in a carefully controlled laboratory environment. Additionally, the first steps have been taken to obtain *in situ* analyses of the surface composition of the ORMAK liner using soft x-ray appearance potential spectroscopic techniques.[3]

Samples of the gold-covered stainless steel liner from ORMAK were analyzed by Auger Electron Spectroscopy (AES). Surface compositions were determined for the samples in the "*as*-received" condition as well as for similar samples subjected to various cleaning techniques and to various environmental conditions. In all the samples studied to date the major surface impurity has been carbon, probably residing on the surface in the form of hydrocarbon. In some of the samples received the carbon concentration on the surface has approached 0.8 atom fraction. Other impurities are present in varying amounts depending on the sample. All samples have exhibited oxygen on the surface and several have been contaminated to a lesser

---

[1]Thermonuclear Division.

[2]Oak Ridge National Laboratory and General Atomic Company, *The Impurity Study Experiment Proposal*, ORNL-TM-4884 (May 1975).

[3]R. L. Park and J. E. Houston, "Soft X-Ray Appearance Potential Spectroscopy," *J. Vac. Sci. Technol.* 11: 1–18 (1974).

degree with iron and sulfur. These results substantiate, in a rather direct way, the vacuum ultraviolet spectroscopic measurements[4] showing the major low-$Z$ plasma impurities to be carbon and oxygen.

Experimental studies of various cleaning techniques have shown that thermal cleaning *in vacuo* is ineffective in reducing the surface concentration of carbon and only slightly effective for oxygen. These studies were carried out in a clean laboratory environment [pressure $\approx 10^{-9}$ torr (0.1 μPa)] at temperatures up to 600°C. The experiments using glow discharge cleaning showed that hydrogen was mildly effective in reducing both carbon and oxygen at the surface but that glow discharge cleaning in oxygen removes essentially all of the carbon. These cleaning techniques, although not completely understood, have been incorporated into routine ORMAK operations. Overnight discharge cleaning in oxygen followed by a short period of hydrogen discharge cleaning reduces the impurity level to a point where increases of 50% or more in the plasma current are routinely obtained.[5]

Several prototype soft x-ray appearance potential spectrometers (SXAPS) have been constructed and tested in an effort to obtain an optimum design for use in connection with the liner impurity studies. The current design is based on the use of a rotatable eight-sided sample mechanically coupled through the vacuum wall so that any face may be alternately exposed to the ORMAK plasma and to the spectrometer. Ion-suppression electrodes are also incorporated in this design to permit operation in the relatively high gas pressure within the liner.

The SXAPS has been installed on ORMAK and is in routine operation. The probe is interfaced with a Digital Equipment Corporation PDP-12 computer, which programs the probe analysis and processes data for further analysis on the ORNL PDP-16 computer. Although reproducible spectra are being obtained, the operation of the probe as well as the

---

[4]R. J. Colchin, "Surface Conditions in the ORMAK Tokamak," pp. 8–9 in *Sixth Annual Conference on Surface Studies* (Host: Union Carbide Corporation Nuclear Division, Y-12 Plant, Oak Ridge, TN, Sept. 10–12, 1974), Y-DA-5966.

[5]Oak Ridge National Laboratory and General Atomic Company, *The Impurity Study Experiment Proposal*, ORNL-TM-4884 (May 1975) p. 8.

data analysis is hindered by the severe electrical noise present in the ORMAK environment. The steps being taken to improve the signal-to-noise ratio include the use of a passive filter to reduce both low- and high-frequency components in the noise spectrum.

A special laboratory facility is being developed to facilitate the surface impurity studies and the overall problem associated with material selection and first-wall design. Work has begun on an intercomparison study between SXAPS and AES in an effort to make the SXAPS techniques more quantative. Additional surface analytical techniques including Electron Spectroscopy for Chemical Analysis (ESCA) and Secondary Ion Mass Spectrocopy (SIMS) will be added to this facility as time and funds permit. These last two spectroscopic techniques will supplement SXAPS and AES by providing additional information on the identity and concentration of surface impurities, particularly with regard to their chemical form.

# 3. COMPATIBILITY STUDIES

J. H. DeVan

Work has been initiated to evaluate the chemical compatibility of fusion reactor blanket and first-wall materials. Potential blanket materials include metallic lithium, $Li_2BeF_4$, and solid lithium compounds. First-wall materials include austenitic stainless steels and refractory alloys based on niobium and vanadium. The compatibility program will assess critical first-wall compatibility problems.

## 3.1 THE REDUCTION OF $Al_2O_3$ IN NIOBIUM-LITHIUM SYSTEMS AT 1000°C — J. E. Selle

Thermodynamic calculations indicate that below 1400°C ceramic insulators of $Al_2O_3$ should not be chemically reduced by niobium or Nb—1% Zr. However, in the case of Nb—1% Zr loops containing lithium,[1] external loop surfaces reacted significantly with $Al_2O_3$ thermocouple insulators at 1100 to 1300°C. Spectrographic and x-ray diffraction analyses showed the reaction zone to be composed of intermetallic compounds with the general formula $Nb_xAl_y$.

Because of the potential requirements for electrical insulators in the controlled Thermonuclear Reactor program, an experiment was conducted to determine the chemical stability of a niobium or Nb—1% Zr wall that adjoins $Al_2O_3$ on one surface and lithium on the other at 1000°C. Three types of $Al_2O_3$ were hermetically sealed in niobium and Nb—1% Zr envelopes, and duplicate envelopes were exposed to vacuum and lithium, respectively. Figure 3.1 shows the test specimen and the test conditions used in the experiments. All lithium tests were conducted in an Nb—1% Zr container.

The data obtained on various samples are summarized in Table 3.1. Distribution coefficients for the partitioning of oxygen and nitrogen were calculated from free energy data and are summarized in Table 3.2.

---

[1] J. H. DeVan and C. E. Sessions, "Lithium Corrosion Studies," *High Temperature Materials Program, Quart. Progr. Rep. Oct. 31, 1964*, ORNL-TM-980, pp. 81—83.

BLANK PAGE

ORNL-DWG 74-13331

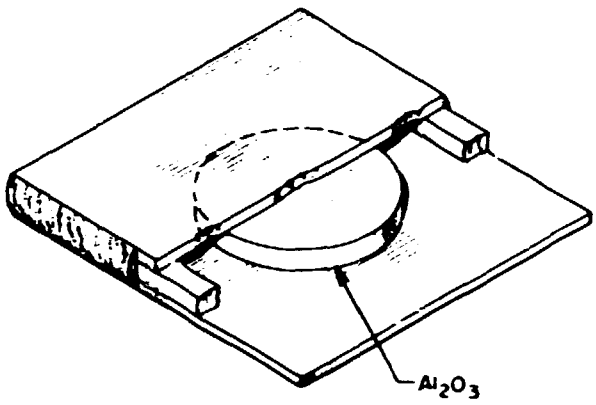


| METAL | INSULATOR | ENVIRONMENT | TEST CONDITIONS |
|---|---|---|---|
| Nb AND Nb-1% Zr | SAPPHIRE<br>LUCALOX<br>99.9% SINTERED $Al_2O_3$ | VACUUM AND LITHIUM | 3000 hr AT 1000°C |

Fig. 3.1. Configuration of Compatibility Test Samples.

Table 3.1. Effect of 3000-hr Exposure to $Al_2O_3$ and Lithium or Vacuum on the Nitrogen and Oxygen Contents and Microhardness of Niobium and Nb–1% Zr

| Location | Test Medium | Content, ppm | | Hardness (DPH) |
|---|---|---|---|---|
| | | Nitrogen | Oxygen | |
| | **Tests on Niobium** | | | |
| At ceramic wafer | Lithium | 19 | 47 | 61.6 |
| | Vacuum | 100 | 427 | 125.9 |
| Away from ceramic | Lithium | 14 | 167 | 63.8 |
| | Vacuum | 70 | 457 | 134.5 |
| | **Tests on Nb–1% Zr** | | | |
| At ceramic wafer | Lithium | 82 | 1126 | 91.2 |
| | Vacuum | 100 | 267 | 91.4 |
| Away from ceramic | Lithium | 89 | 51 | 103.1 |
| | Vacuum | 96 | 803 | 103.8 |

Table 3.2. Calculated Distribution Coefficients for Oxygen and Nitrogen Between Niobium or Zirconium and Lithium

| | Distribution Coefficient Metal/Li | |
|---|---|---|
| | Niobium | Zirconium |
| Oxygen | $2.13 \times 10^{-6}$ | 2.92 |
| Nitrogen | 2460.7 | $1.746 \times 10^{9}$ |

The distribution coefficient, $K_D$ is defined as

$$K_D = C_m / C_{Li} \quad (1)$$

where $C_m$ and $C_{Li}$ are the concentrations in weight percent of the nonmetallic elements in the metal and the lithium, respectively.

With one exception, the data of Table 3.1 correlate with the distribution coefficients. The exception is nitrogen in niobium. Table 3.2 predicts that the metal should getter nitrogen from the lithium. However, the nitrogen content of the niobium sample decreased in lithium. An explanation of this observation is found in the fact that the niobium and Nb–1% Zr samples were run in the same container, also of Nb–1% Zr. The large amount of zirconium present in the system resulted in removal of nitrogen not only from the lithium, but also from the niobium.

Reactions of the type

$$2Nb + 3Al_2O_3 \rightarrow 2NbAl_3 + 9\ O(\text{in Nb}) \quad (2)$$

$$2Zr + 3Al_2O_3 \rightarrow 2ZrAl_3 + 9\ O(\text{in Zr}) \quad (3)$$

$$9\ O(\text{in Nb or Zr}) \rightarrow 9\ O(\text{in Li}) \quad (4)$$

are suggested by the data. Reaction (3) coupled with a distribution coefficient of 2.92 for oxygen in zirconium explains the high value of oxygen at the ceramic wafer for Nb–1% Zr in lithium.

These data suggest that for systems where electrical insulators are required, special consideration must be given to the thermodynamic stability of the insulator if metallic lithium also is present.

## 3.2 SOLID MODERATOR STUDIES — J. E. Selle

The solid moderator concept for a Controlled Thermonuclear Reactor (CTR) requires a lithium-bearing compound for tritium breeding. Work was initiated to develop methods for distributing lithium-bearing compounds throughout reactor-grade graphite.

Lithium compounds were surveyed, and the more stable compounds are summarized in Table 3.3 along with pertinent data such as molecular weight, structure, melting point, density, and lithium content. The compounds $Li_2Co_3$ and $LiNO_3$ are included because of their potential ease of solution in a carrier solvent and subsequent dissociation into higher melting compounds. Calculations were made to determine which compounds could produce enough lithium in the system. If 1% is the lower limit and 100% of the voids in reactor-grade graphite are filled, only $LiNO_3$, $Li_2CO_3$, $LiFeO_2$, $LiAlO_2$, and $Li_2O$ could be useful.

Graphite samples were impregnated by evacuating a chamber containing the graphite and backfilling with a saturated lithium-bearing solution. This was then followed by drying and bakeout steps. This procedure was repeated until saturation or maximum weight gain occurred. Several grades of graphite were used: ATJ ($\rho$ = 1.73 g/cm$^3$), AGOT ($\rho$ = 1.69 g/cm$^3$), AXZ-5Q ($\rho$ = 1.56 g/cm$^3$), an experimental graphite ($\rho$ = 1.25 g/cm$^3$), and a graphite felt ($\rho$ = 0.24 g/cm$^3$).

Essentially no water is absorbed by AXZ graphite in the evacuation and backfill method, although water uptake is possible with AGOT. About 58% of the voids were filled when water was used. The difference is associated with pore size rather than density, since AGOT is more dense than AXZ graphite. AGOT graphite is made from larger (0.030 in. max) coke particles than the others.

A summary of $LiNO_3$ uptake by the various grades of graphite is given in Table 3.4. The amount of lithium uptake increases as the graphite density decreases. Also, 100% filling of the voids was not achieved. To achieve an uptake of greater than 1 at.% Li with $LiNO_3$, graphite less dense than 1.[illegible] g/cm$^3$ must be used. Theroretically, graphite with density of less than 1.78 g/cm$^3$ could be used. However, inaccessibility of all of the voids, variable pore size, and clogging of the smaller pores decreases this to a practical limit of about 1.5 g/cm$^3$.

Table 3.3 Solid Compounds of Lithium

| Compound | Molecular Weight | Structure | Melting Point (°C) | Density ($g/cm^3$) | Lithium (at. %) |
|---|---|---|---|---|---|
| $Li_2O$ | 29.88 | Cubic | 1570 | 2.01 | 66.7 |
| $LiAl_5O_8$ | 269.85 | Spinel | 1950 | 3.64 | 7.1 |
| $LiAlSi_2O_6$ | 186.10 | Spodumene | 1450 | 2.38 | 10 |
| $LiAlSiO_4$ | 126.01 | Phenacite | ? | 2.035 | 14.3 |
| $Li_2Si_2O_5$ | 150.0 | Petalite | 1034 | 2.44 | 22.2 |
| $LiAlO_2$ | 65.9 | Rhombohedral | 1700 | 3.40 | 25 |
| $LiFe_5O_8$ | 414.14 | Spinel | 1600 | 4.62 | 7.1 |
| $LiFeO_2$ | 94.78 | NaCl | 1618 | 4.435 | 25 |
| $Li_2CO_3$ | 73.89 | Monoclinic | 720 | 2.07 | 33.3 |
| $LiNO_3$ | 68.95 | Trigonal | 255 | 2.38 | 20 |

Table 3.4 Graphite Impregnation with $LiNO_3$ from Ethyl Alcohol Solution

| Graphite Type | Graphite Density ($g/cm^3$) | Maximum Lithium Content, at. % | | Percent of Theoretical |
|---|---|---|---|---|
| | | Found | Theoretical | |
| ATJ | 1.73 | 0.20 | 1.14 | 17.54 |
| AGOT | 1.69 | 0.37 | 1.24 | 29.84 |
| AXZ-5Q | 1.56 | 0.80 | 1.63 | 49.08 |
| Experimental | 1.25 | 1.50[a] | 2.89 | 51.90 |
| Graphite Felt | 0.24 | 13.0 | 23.58 | 55.13 |

[a]Weight loss due to disintegration of the graphite in the solution.

The effect of sample size, if any, is small, at least in the sample size range from 3/16 to 3/8 in. (4.8–9.5 mm).

An overpressure of 90 psig (0.62 MPa gage) increases the percentage of voids filled by about 16% for both ethyl alcohol and water. The effect of an overpressure on the net $LiNO_3$ impregnation was not determined.

## 3.3 SALT SYSTEMS — J. R. Keiser and J. E. Selle

Design and fabrication of a type 316 stainless steel thermal-convection loop has been completed, and the heaters have been installed. The loop will be operated with $Li_2BeF_4$ salt at a maximum temperature of 650°C. The system is equipped with electrochemical probes to determine the effects of changes in the salt composition on the oxidation potential of the salt. The loop is expected to be in operation about August 1, 1975.

## 3.4 LITHIUM-STAINLESS STEEL CORROSION STUDIES — J. E. Selle

Serious consideration is being given to the use of type 316 stainless steel as the primary containment material for a lithium-cooled Controlled Thermonuclear Reactor (CTR).[2] Therefore, an extensive literature search[3] was conducted on the compatibility of ferrous metals with lithium, with the emphasis on austenitic stainless steels. The results of this literature search were then used to plan a detailed compatibility program.

Correlations of previous corrosion studies with lithium are complicated by variations in lithium purity, alloy treatment, flow rates, and lithium handling procedures. The available data on corrosion rate versus reciprocal temperature for various stainless steel loops are summarized in Fig. 3.2. The corrosion rates of gettered and ungettered lithium systems are comparable at 800°C. However, the corrosion rate of gettered systems appears to decrease faster with decreasing temperature. Gettered systems also show less intergranular attack. The data suggest an activation energy of about 60 kcal/mole (250 kJ/mole) for titanium-gettered systems,

---

[2]B. Badger et al., *UWMAK-I, A Wisconsin Toroidal Fusion Reactor Design*, UWFDM-68, University of Wisconsin (November 1973).

[3]J. H. DeVan, J. E. Selle, and A. E. Morris, *Review of Lithium — Iron-Base Alloy Corrosion Studies*, ORNL-TM-4927 (to be published).

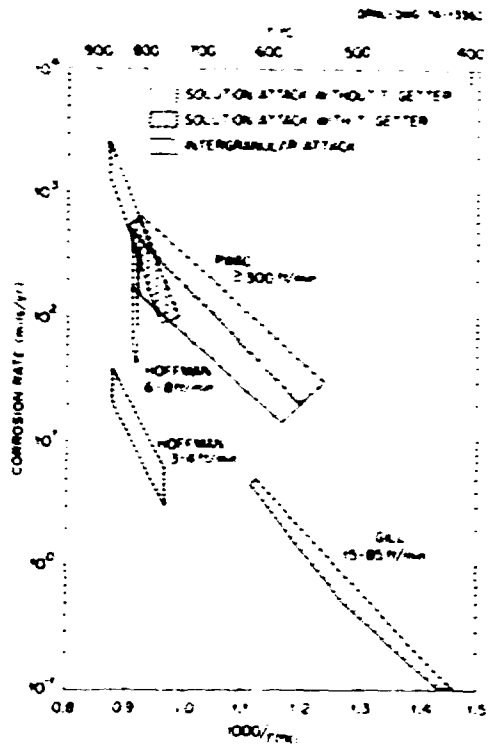

Fig. 3.2. Summary of Available Loop Data for Austentic Stainless Steels in Lithium. To convert: 1 mil = 25.4 μm, 1 ft/min = 5.1 mm/sec.

compared with about 20 kcal/mole (80 kJ/mole) for ungettered systems. This can be explained by the work of Gill et al.,[4] who showed that the rate of stainless steel dissolution is controlled by solid-state diffusion at the surface and not by solution in the liquid. Solid-state diffusion-controlled processes would be expected to have activation energies in the range 60 to 70 kcal/mole (250–300 kJ/mole), while liquid-phase diffusion or solution-controlled processes would be expected to have activation energies about 20 kcal/mole (80 kJ/mole). This suggests that gettered-lithium mass transfer is controlled by solid-state diffusion while that by nitrogen-bearing lithium is liquid-phase diffusion controlled. Grain boundary grooving experiments[5] with iron in ungettered lithium gave an activation energy of 18 kcal/mole (75 kJ/mole).

---

[4]W. W. Gill et al., *AIChE J.*, 6(1): 139 (1960).

[5]D. L. Olson and W. L. Bradley, *Liquid Lithium Corrosion Research*, COO-2313-2 (1975).

# 4. MAGNET DEVELOPMENT[1]

## 4.1 PREPARATION AND EXTRUSION OF MULTIFILAMENTARY NIOBIUM-TITANIUM CONDUCTOR BILLETS – R. E. McDonald and W. A. Fietz[2]

In cooperative program with industry, 20 billets were designed and assembled. Fourteen contained no superconductors. These were "dummy" billets to evaluate methods of stacking to achieve the best packing density. The dummy billets were not extruded, but were compacted by hot isostatic pressing or rotary forging and sectioned transversely and longitudinally to evaluate the billet preparation techniques. The remaining billets were assembled with niobium-titanium stacking elements in a standard conductor configuration. Two were instrumented with thermocouples and used to evaluate billet preheating techniques before actual extrusion; the remaining billets were extruded (using the instrumented billet for reference temperatures) and drawn to final conductor size to be used for critical current measurements and evaluation.

The results of this study were:

1. Hexagonal stacking elements are essential to producing a dense billet.

2. Internally contoured billet cans improve packing density, but filler rods to fill the intertices give satisfactory results.

3. Rotary forging is not acceptable for compaction.

4. Hot isostatic pressing can result in an extremely dense billet if hexagonal stacking elements, fully annealed billet jackets, and filler rods are used and pressed under argon at 1200°F (649°C) at 15,000 psi (103 MPa).

5. Fast billet heating can be achieved both in the salt bath and by 60-Hz induction heating. The induction heating gives a more uniform temperature distribution during the total heating cycle. The salt reaches a uniform heat distribution at approximately two-thirds the selected temperature (1200°F).

---

[1]Funding provided by the Superconducting Magnet Development Program of the Thermonuclear Division.

[2]Thermonuclear Division.

BLANK PAGE

6. Poorly assembled and low-packing-density billets will result in highly nonuniform filament size distribution, which, in turn, leads to poor critical current performance.

7. Billet yields can be increased as much as 16% by contouring the stacking elements within the billets.

8. Using thermal tabs within the billet showed thermal excursions during extrusion, but not quantitatively.

In the production of the multifilamentary niobium-titanium conductors, billet stacking and extrusion were considered to be critical and the extrusion to be among the most critical in the total process.

Figure 4.1 shows cross sections of 156-filament extruded wirebars. In (a) the billet was designed, stacked, and compacted by use of the knowledge gained from the investigation. In (b) is a wirebar from a billet that was poorly designed and poorly stacked.

The thermal tab concept was used in the billet stacking for evaluating the temperature excursions caused by adiabatic heating during billet upset and extrusion. Carbon steel (Fe–0.06% C) was chosen because its microstructure after extrusion should reveal the temperature to which the steel had been exposed. However, the effect of pressure on the phase change in the steel confuses the temperature effects. We could see microstructural changes but not identify the temperatures leading to them.

Two experimental billets were prepared for extrusion at ORNL. The billets were assembled from annealed copper-nickel cans, copper matrix, and 13 nickel rods. One billet had a copper-nickel nose and the second billet had a copper nose. The billets were extruded under the same conditions as industry had used, 1200°F (649°C) at a 16/1 reduction ratio. The sectioned extrusions revealed a microstructure in the nickel typical of 800°F (427°C) at 1 atm (0.1 MPa). The microstructures also revealed that the copper-nickel-nosed billet produced a more uniform grain structure throughout the total length of the extrusion than the copper-nosed billet. The difficult interpretation is the effect of dynamic pressure on the physical properties of the materials.

A quench tube was designed and fabricated to quench the extrusion as it left the die [within 4 in. (0.1 m) of exit]. Two more billets were

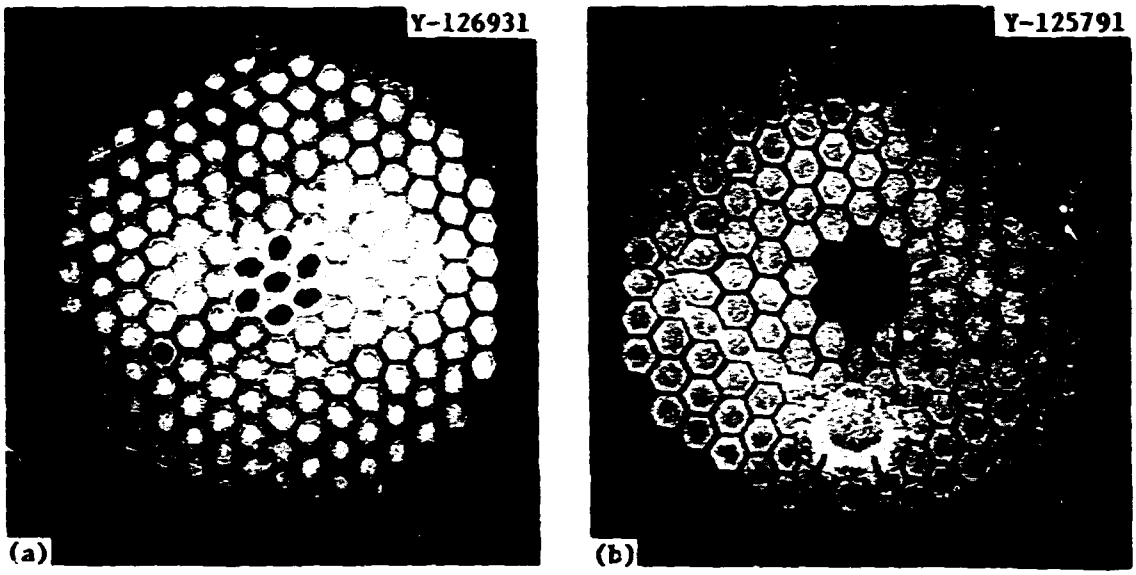


Fig. 4.1. Cross Sections of 156-Filament Wirebars. 2.75×. (a) Made from properly stacked billet. (b) Made from poorly designed and poorly stacked billet.

fabricated; these billets were nearly identical to the first two, but contained various metal thermal tabs within all but four of the nickel rods. The extrusions were under the identical conditions of the other two billets. The instant-quench tube is a reality, and the microstructures of the quenched extrusions are being investigated.

Work will continue on the evaluation of thermal tabs and billet designs in order to produce wirebar that will make wire of greater consistency.

## 4.2 PROCUREMENT OF NIOBIUM-TITANIUM ALLOY ROD — R. J. Beaver

One of the important alloys under consideration for use as filaments in the copper-bearing superconductive wire for fusion reactor magnets is a niobium-base alloy containing titanium. Of particular interest in the ORNL program are those alloys with nominal concentrations of 45 and 48 wt % Ti.

The primary objective of this procurement program is to develop industrial capability for providing 0.5-in. (13-mm) Nb-Ti alloy rod to ERDA contractors under procurement specifications that provide for control of manufacturing requirements and verification of the quality of the finished product. The 0.5-in.-diam rods serve as the basic wrought

material, which is subsequently reduced to an appropriate size, jacketed with OFE copper, assembled into an OFE cylinder, and processed into small-diameter wire containing the Nb-Ti alloy as filaments. It is of primary importance that the quality of these 0.5-in.-diam rods with respect to composition; composition variations; freedom from cracks, laminations, and detrimental inclusions; mechanical properties; and grain size be controlled.

Two specifications were developed, ORNL-TD-SC-1 for the Nb-45 wt % Ti alloy and ORNL-TD-SC-2 for the Nb-48 wt % alloy. Except for the titanium concentration requirement these specifications are identical. The basic technical requirements of ORNL-TD-SC-1 are listed as follows:

Composition:

| | |
|---|---|
| Ti | 45 ± 2 wt % |
| C | 200 ppm, max |
| O | 1000 ppm, max |
| N | 150 ppm, max |
| Fe | 200 ppm, max |
| Ta | 1000 ppm, max |
| Ni | 125 ppm, max |

Hardness: <170 DPH

Grain Size: ASTM 6 or finer

Defects: Freedom from cracks, laminations, and other ruptures

Inclusions: Freedom from inclusions larger than 0.013 in. (0.33 mm) (equivalent diameter)

The latter two requirements relating to the integrity of the rods are determined by qualified ultrasonic and liquid-penetrant procedures. These technical requirements are based on the past experience of two suppliers of superconductivity wire, MCA and Supercon, and negotiations with potential suppliers of the niobium-titanium before contract award. These suppliers included Teledyne, Wah Chang Albany, Kawecki-Berylco Industries (KBI), and Fansteel. The quality assurance requirements are based on the ERDA RDT Standard, RDT F 2-4T, *Quality Verification Program Requirements.*

The initial procurement consisted of processing 2041 lb (926 kg) of the Nb-45 wt % Ti alloy and 1906 lb (865 kg) of the Nb-48 wt % Ti alloys.

Of these alloys, 1866 lb (846 kg) represents 401 lengths of high-quality 0.5-in.-diam (13-mm) rod completely tested and inspected. The balance represents semifinished 1.6-in.-diam (41-mm) bar as stock for production of additional 0.5-in.-diam rod when necessary. Surveillances of the manufacturing facilities and quality assurance programming of the two suppliers of this material, Teledyne Wah Change Albany and Kawecki-Berylco, were conducted during the period these items were manufactured. These reviews revealed that both these suppliers have the capabilities to manufacture production quantities of niobium-titanium alloy bar and rod and utilize acceptable quality assurance programming in their manufacturing and inspection activities.

The secondary purpose of this procurement program is to characterize heats of material to determine variations in chemical, mechanical, and metallurgical properties within each heat as well as heat-to-heat variations. The assessment exclusive of tensile properties is based on statistical evaluation of results from representative samples cut from 0.5-in.-diam rods made from known positions in the casting. In any comparison between the Nb–45 wt % Ti alloy rods manufactured by Teledyne Wah Chang Albany and Kawecki-Berylco, conclusions must be reserved because of the limited quantity supplied by Kawecki-Berylco (11 pieces) and the fact that the pieces came from several castings. All 205 rods produced by Wah Chang were from the same casting. The mechanical properties based on certified results of the two suppliers are compared in Table 4.1. The most noticeable characteristic is the higher reduction of area values representing the Kawecki-Berylco rods. This difference is probably associated with differences in annealing practices by these suppliers.

Investigations of variations within a heat were confined to Teledyne Wah Change Albany Heat 590522Q and Kawecki-Berylco Lot 8787, representing the Nb–45 wt % Ti alloy. No work was initiated on the Nb–48 wt % Ti alloys. Wah Chang Heat 590522Q is typified by the following characteristics.

1. The variations in the titanium concentration are illustrated by Table 4.2. Statistical analyses indicated that all but 0.3% of the 205 rods will comply with the 45 ± 2 wt % Ti requirement.

Table 4.1. Mechanical Properties of Niobium-Titanium Alloy 0.5-in.-Diam (13-mm) Rod

| Supplier | Strength, psi (MPa) | | Elongation (%) | Reduction of Area (%) | Hardness (VHN) |
|---|---|---|---|---|---|
| | Ultimate Tensile | Yield | | | |
| | | Nb-45 wt % Ti Alloy | | | |
| Wah Chang | 68,000 (469) | 68,000 (469) | 25 | 65 | 140 to 142 |
| | 69,000 (476) | 69,000 (476) | 25 | 63 | 140 to 142 |
| Kawecki-Berylco | 58,000 (400) | 54,600 (376) | 32 | 92 | 125 to 140 |
| | 58,000 (400) | 55,800 (385) | 32 | 93 | 125 to 143 |
| | 57,200 (394) | 53,900 (372) | 34 | 92 | 125 to 139 |
| | | Nb-48 wt % Ti Alloy | | | |
| Wah Chang | 72,000 (496) | 72,000 (496) | 24 | 64 | 135 to 149 |
| | 71,000 (490) | 71,000 (490) | 24 | 65 | 135 to 149 |
| Kawecki-Berylco | 57,200 (394) | 54,900 (379) | 38 | 90 | 123 to 143 |
| | 59,000 (407) | 57,000 (393) | 31 | 87 | 119 to 151 |
| | 55,200 (381) | 52,900 (365) | 28 | 91 | 123 to 153 |

Table 4.2. Variations in the Concentrations of Ti, O, C, and N Among 200 0.5-in.-Diam (13-mm) Rods Made from a Single Casting, Teledyne Wah Chang Albany Heat 59022Q Nb-45 wt % Ti

| Location[a] (%) | Titanium Content (wt %) | Interstitial Content, ppm | | |
|---|---|---|---|---|
| | | Oxygen | Carbon | Nitrogen |
| 0 | 46.37 | 690 | 90 | 20 |
| 5 | 45.99 | 680 | 102 | 26 |
| 20 | 45.91 | 660 | 83 | 22 |
| 35 | 45.86 | 680 | 108 | 24 |
| 45 | 45.00 | 720 | 87 | 23 |
| 60 | 45.12 | 660 | 72 | 24 |
| 75 | 44.64 | 640 | 76 | 24 |
| 85 | 45.13 | 640 | 85 | 15 |
| 95 | 45.10 | 625 | 75 | 12 |
| 100 | 46.48 | 624 | 73 | 23 |

[a]Relative distance from top of casting.

2. The variations in the important interstitials, oxygen, carbon, and nitrogen, are illustrated in Table 4.2.

3. The standard deviations associated with the variations in the chemical elements specified and the variations in the zirconium and tin tramp impurities found in this material are listed in Table 4.3 along with the average concentrations of these elements.

Table 4.3. Composition Characteristics of Niobium-Titanium Rods

| Chemical Element | ORNL-TD-SC-1[a] Requirements | Average Concentration[a] (Standard Deviation) | |
|---|---|---|---|
| | | Teledyne Wah Chang Heat 590522Q | Kawecki-Berylco Lot 8787 |
| Ti | 45 ± 2 | 45.56 (0.64) | 44.47 (0.14) |
| C | 200 | 85 (12) | 104 (14) |
| O | 1000 | 662 (21) | 543 (46) |
| N | 150 | 21 ( 5) | 65 (10) |
| Fe | 200 | 84 (13) | 113 (26) |
| Ta | 1000 | 150 (28) | 191 (37) |
| Ni | 125 | 16 (18) | 2 |
| Zr | Not Specified | 150 | 7 ( 5) |
| Sn | Not Specified | 58 (17) | 6 ( 2) |

[a]Titanium in wt %, other elements in ppm (ppm max in specification).

4. The microstructure of the transverse cross section of rod 1 shows in Fig. 4.2 typifies the "coring" effect generally observed in these rods and the differences in the grain structure of the periferal region and the cored region. The microstructure at higher magnification, as illustrated in Fig. 4.3 reveals the presence of grain boundary precipitates of eutectic structure.

5. The "cored" structure appears to be related to variations in titanium concentration as shown by Fig. 4.4.

6. The average grain size of the rods in this heat is ASTM 7, with a standard deviation of 0.6.

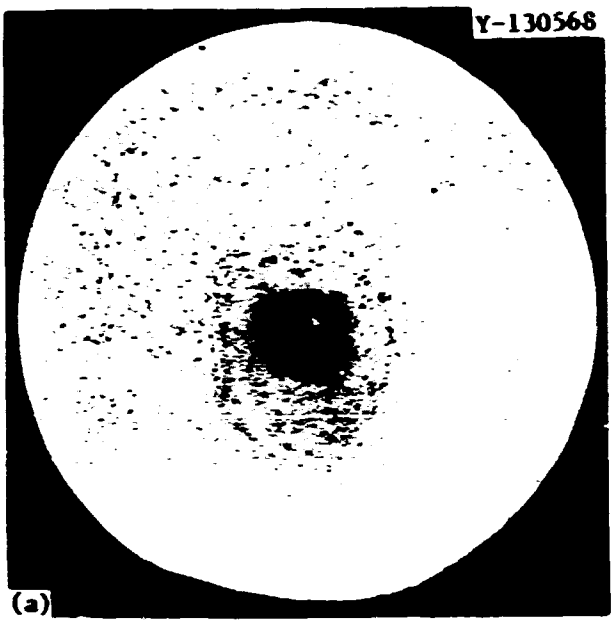




Fig. 4.2. Pronounced "Coring" Effect in Rod 1 of Teledyne Wah Chang Albany Heat 5905220 Nb–45 wt % Ti. Etched with 50 $H_2O$-25 $HNO_3$-15 $H_2SO_4$-10 HF. (a) 7×. (b) Central region at 200×. (c) Periferal region at 200×.

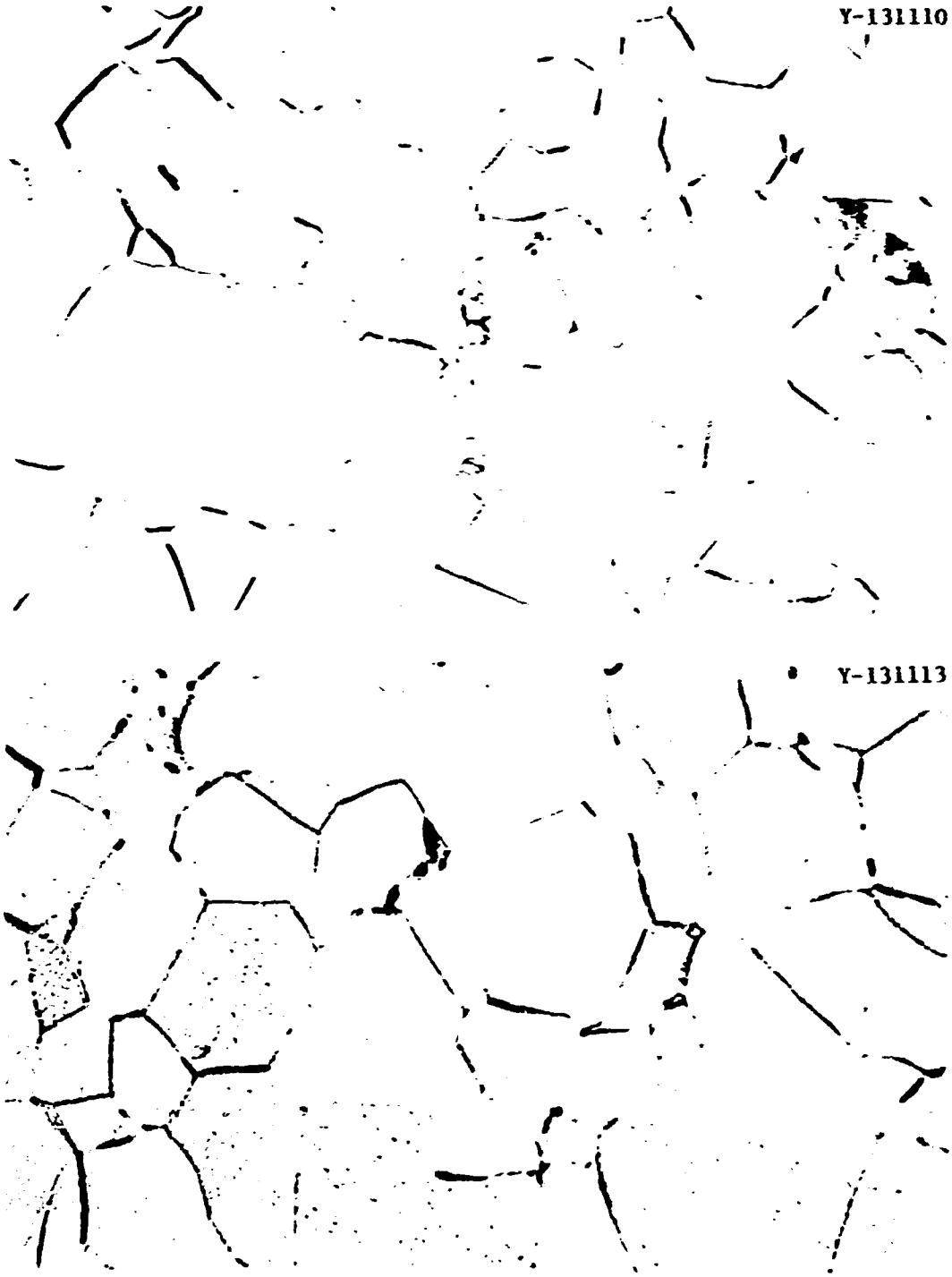


Fig. 4.3. Grain Boundary Precipitates in Microstructure of Teledyne Wah Chang 0.5-in.-Diam (13-mm) Rods Heat 59022Q Nb–45 wt % Ti. Etched with 50 $H_2O$–25 $HNO_3$–15 $H_2SO_4$–10 HF. 1000×.

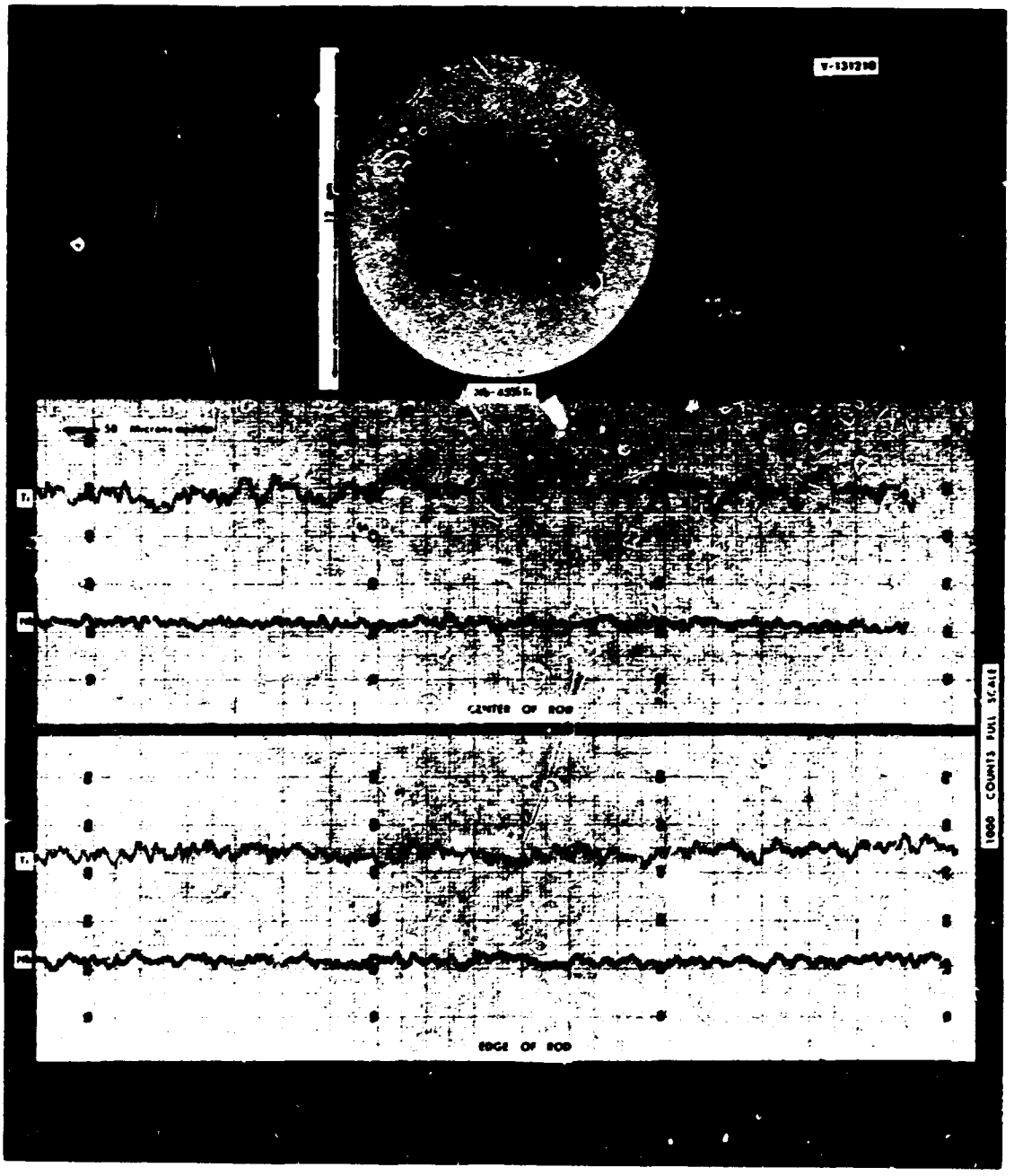


Fig. 4.4. Composition Variation in Wah Chang Niobium-Titanium Alloy Determined by Microprobe Continuous Line Scans.

7. The average hardness of the rods in this heat is 129 DPH, with a standard deviation of 7 DPH.

Sections of rods of Kawecki-Berylco Lot 8787 showed results similar to the Wah Chang rods. "Coring" is present but less intense. The average grain size is ASTM 8, with a standard deviation of 1.3. The average hardness is 126 DPH, with a standard deviation of 10 DPH. A slight amount of precipitate appeared to exist at the grain boundaries of the Kawecki-Berylco rods but to an extent significantly less than observed in the Wah Chang material. The standard deviations associated with the variations in the chemical elements specified and the variations in zirconium and tin impurities are listed in Table 4.3. A chemical distinction between the Wah Change material and the Kawecki-Berylco material appears to exist by the noticeably higher concentration of zirconium and tin in the Wah Chang material.

## 4.3 STRESS EFFECTS IN SUPERCONDUCTORS — C. C. Koch, D. S. Easton, and S. B. Waters

Our task is to determine the influence of mechanical stress on superconducting composites. This work is directly related to the Conductor Tests and Selection subprogram but also provides input to the Structural Analysis and Materials Tests and the Coil Test and Evaluation subprograms. Our goal is to supply accurate data on the influence of mechanical stress at 4.2 K in transverse magnetic fields on the current-carrying capacity of commercial superconductors of interest to the Superconducting Magnet Development Program. The work in the reporting period can be divided into two parts: (1) The collection of mechanical properties data at 4.2 K (and 298 and 77 K) on a variety of conductors, and (2) design and construction of apparatus to allow the *in situ* measurements of $J_c$ under stress at 4.2 K in transverse magnetic fields to 70 kOe.

The tensile measurements at 4.2 K have revealed pseudoelastic behavior, which may have implications on magnet performance. In brief, a nonlinear elastic region is observed in niobium-titanium conductors and composites, which on reducing the stress results in a hysteresis loop and therefore heat generation. The severity of this effect varies with conductor type, geometry, and possibly composition. Serrated stress-strain curves are also observed and audible clicks are heard; these presumably represent

stress-induced formation of martensitic plates and/or twins. These serrations (load drops) are also a source of heat. An example of both a hysteresis loop and serrated load drops are shown in Fig. 4.5 for a mixed-matrix composite. Details of some of the work on the pseudoelastic behavior of Nb-Ti/Cu composites, Nb-Ti filaments, and Nb-Ti tensile specimens have been reported.[3,4]

---

[3]D. S. Easton and C. C. Koch, "Tensile Properties of Superconducting Composite Conductors and Nb-Ti Alloys at 4.2 K," paper presented at the International Symposium on Shape Memory Effects and Applications at the 7th Annual TMS-AIME Spring Meeting, May 18–22, 1975 at the University of Toronto, Ontario, Canada.

[4]D. S. Easton and C. C. Koch, "Mechanical Properties of Superconducting Nb-Ti Composites," presented at the 1975 International Cryogenic Materials Conference, Queens University, Kingston, Ontario, Canada, July 22–25, 1975.

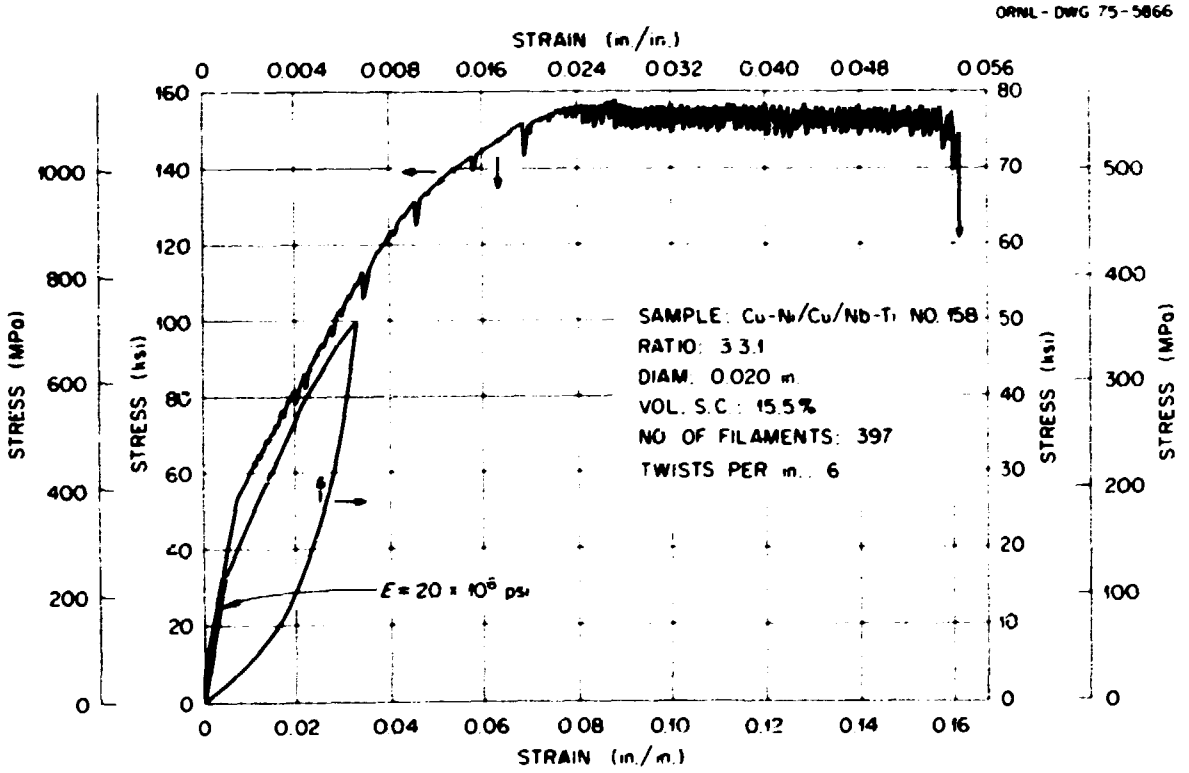


Fig. 4.5. Stress-Strain Behavior of Mixed-Matrix Composite Conductor.

Some characteristics of the various composites that we have tested are listed in Table 4.4, and various tensile property values are given in Table 4.5. Besides these composites we have tested niobium-titanium filaments that had been chemically removed from various composites, tensile samples machined from rods of Nb–45 wt % Ti and Nb–48 wt % Ti, as well as pure copper, niobium, and titanium as checks on our techniques.

Table 4.4. Some Characteristics of Various Superconducting Composites

| Sample | Size (mm) | Ratio Cu-Ni to Cu to Nb-Ti | Nb-Ti (vol %) | Number of Filaments | Filament Diameter (μm) | Twists per cm |
|---|---|---|---|---|---|---|
| 1 | 1.30 × 3.12 | 0:3.6:1 | 22 | 15 | 279 | None |
| 2 | 1.44 × 2.90 | 0:2.8:1 | 26 | 18 | 279 | None |
| 3 | 1.30 × 3.12 | 0:2.3:1 | 30 | 24 | 203 | 0.13 |
| 4 | 1.32 × 6.68 | 0:3.4:1 | 22.7 | 84 | 188 | 0.039 |
| 5 | 0.99 × 10.06 | 0:3.4:1 | 22.7 | 84 | 173 | 0.031 |
| 6 | 0.81 × 12.09 | 0:3.4:1 | 22.7 | 84 | 183 | 0.020 |
| 7 | 0.76 diam | 3:3:1 | 13.4 | 397 | 14.0 | 1.2 |
| 8 | 0.76 diam | 3:3:1 | 13.4 | 397 | 14.0 | 1.6 |
| 9 | 0.76 diam | 3:3:1 | 13.4 | 397 | 14.0 | 2.2 |
| 10 | 0.51 diam | 3:3:1 | 13.4 | 397 | 9.4 | 1.6 |
| 11 | 0.51 diam | 3:3:1 | 13.4 | 397 | 9.4 | 2.4 |
| 12 | 0.51 diam | 3:3:1 | 13.4 | 397 | 9.4 | 3.2 |
| 13 | 0.38 diam | 1.5:2:1 | 22.2 | 156 | 14.5 | 2.8 |
| 14 | 0.38 diam | 1.5:2:1 | 22.2 | 156 | 14.5 | 3.2 |
| 15 | 0.38 diam | 1.5:2:1 | 22.2 | 156 | 14.5 | 4.3 |
| 16 | 0.51 diam | 1.5:2:1 | 22.2 | 156 | 19.0 | 2.0 |
| 17 | 0.51 diam | 1.5:2:1 | 22.2 | 156 | 19.0 | 2.4 |
| 18 | 0.51 diam | 1.5:2:1 | 22.2 | 156 | 19.0 | 3.2 |

## Table 4.5. Tensile Properties of Superconducting Composites[a]

| Sample | Temperature (K) | Ultimate Tensile Strength, MPa | | Total Elongation (%) | Reduction of Area (%) | Young's Modulus, GPa | | Hysteresis Loop[b] |
|---|---|---|---|---|---|---|---|---|
| | | Experimental | Rule of Mixture | | | Experimental | Rule of Mixture | |
| 1 | 300 | 366 | 400 | 15 | -- | 93.1 | 104.1 | Yes |
| 2 | 300 | 428 | 434 | 17 | 16 | 101.4 | 102.8 | Yes |
| | 77 | 690 | 704 | 26 | -- | -- | 105.5 | Yes |
| | 4.2 | 791 | 921 | 2 | 14 | 117.2 | 108.3 | Yes |
| 3 | 300 | 400 | 462 | 17 | -- | 110 | 102 | -- |
| 4 | 300 | 510 | 407 | 1.8 | -- | 96.6 | 104.1 | VS |
| | 4.2 | 766 | 847 | 2.7 | -- | 110.3 | 109.7 | VS |
| 5 | 300 | 538 | 462 | 9.0 | -- | 103.4 | 104.1 | VS |
| | 4.2 | 759 | 847 | 2.2 | -- | 110.3 | 109.7 | VS |
| 6 | 300 | 538 | 462 | 2.0 | -- | 96.6 | 104.1 | VS |
| | 4.2 | 828 | 847 | 2.5 | -- | 110.3 | 109.7 | VS |
| 7 | 4.2 | 1055 | 813 | 7.7 | 11.2 | -- | 111.7 | Yes |
| 8 | 4.2 | -- | 813 | 9.2 | 11.9 | -- | 111.7 | Yes |
| 9 | 4.2 | -- | 813 | -- | 11.1 | -- | 111.7 | Yes |
| 10 | 4.2 | 1117 | 813 | 5.7 | 21.3 | 117.2 | 111.7 | Yes |
| 11 | 4.2 | 1062 | 813 | 5.0 | 17.8 | 117.9 | 111.7 | Yes |
| 12 | 4.2 | 1055 | 813 | 8.8 | -- | -- | 111.7 | Yes |
| 13 | 4.2 | 1211 | 926 | 4.6 | 18.0 | -- | 122.8 | Yes |
| 14 | 4.2 | 1227 | 926 | 5.1 | 15.8 | -- | 122.8 | Yes |
| 15 | 4.2 | 1166 | 926 | 5.9 | 20.4 | 117.2 | 122.8 | Yes |
| 16 | 4.2 | 1179 | 926 | 5.3 | 11.0 | -- | 122.8 | Yes |
| 17 | 4.2 | 1132 | 926 | 5.5 | 14.7 | -- | 122.8 | Yes |
| 18 | 4.2 | 1141 | 926 | 6.5 | 15.7 | -- | 122.8 | Yes |
| Nb 6a | 300 | 1034 | | 1.2 | | 82 | | |
| At. [illegible] | 77 | 1724 | | 2.4 | | 82.4 | | |
| | 4.2 | 2207 | | 3.8 | | 82.8 | | |
| Cu | 300 | 221 | | 45[c] | | 110 | | |
| | 77 | 345 | | 62[c] | | 114 | | |
| | 4.2 | 448 | | 74.0 | | 117 | | |
| Cu 30 Ni | 300 | 400[c] | | 42[c] | | 152[c] | | |
| | 77 | 621[c] | | 52[c] | | 159[c] | | |
| | 4.2 | 724[c] | | 48[c] | | 160[c] | | |

[a] -- = Not measured.

[b] VS = Very small.

[c] Data from R. P. Reed and R. P. Mikesell, [illegible] 92 (1966).

In general, for the composites we have tested we observe large hysteresis (pseudoelastic) effects in composites with straight Nb-Ti filaments and in small-diameter mixed-matrix composites with tight twist pitches. A series of flat conductors with "loose" twist pitches (≈0.1 twists/in.), and aspect ratios (thickness to width) of 5 to 15 exhibited much smaller pseudoelastic effects and followed more conventional mechanical behavior at 4.2 K. While this behavior is not completely understood, it is likely that the differing stress state is the twisted filaments is responsible.

The efforts to design and construct an apparatus for *in situ* $J_c$ vs $H$ measurements under stress have been completed, and it is shown in Fig. 4.6.

This year's work has demonstrated pseudoelastic behavior and serrated stress strain curves (which are potential sources of heat generation) in Nb-Ti composite conductors. While it is clear that the origin of this behavior is mainly attributable to the Nb-Ti filaments, the severity of this behavior critically depends on the type and geometry of the composite conductor. To what extent these mechanical effects will influence superconducting performance will be demonstrated in an apparatus that will be operational in FY 1976.

## 4.4 ANALYSIS OF EDDY-CURRENT PHENOMENA IN THERMONUCLEAR EXPERIMENTS — C. V. Dodd and W. E. Deeds[5]

Because of the magnitude of the magnetic fields involved in thermonuclear experiments, eddy-current phenomena can have very serious effects on a thermonuclear experiment. If the experiment is not properly designed, forces generated in the start-up and shutdown of a large electromagnet may damage the apparatus, and the power dissipated in conductors can drive the superconducting coils normal. The voltages generated in a second coil by the current in the first coil being dumped may cause the second coil to inadvertently dump its current.

Many of the techniques that have been used to analyze eddy-current phenomena applied to nondestructive testing may also be used to analyze the various induction interactions in thermonuclear experiments. In

---

[5]Consultant from the University of Tennessee.

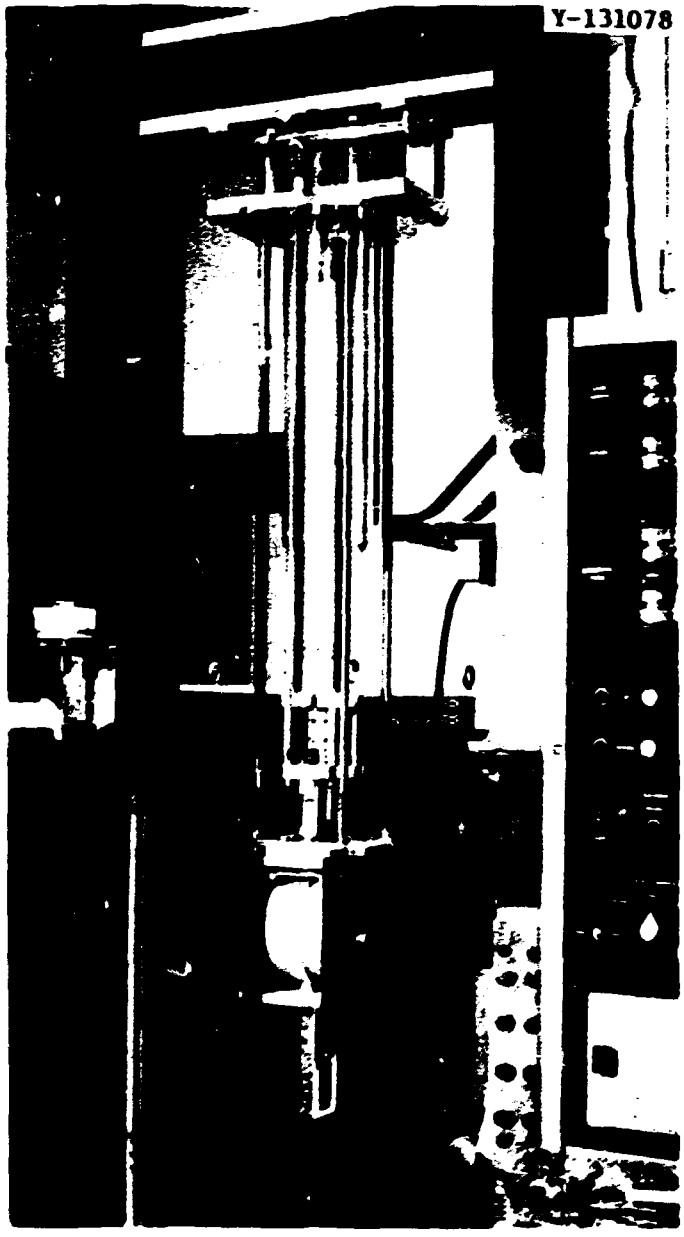


Fig. 4.6. *In-Situ* Low-Temperature Tensile Test Apparatus.

addition, much of the equipment and apparatus can be used for both nondestructive and thermonuclear eddy-current experiments.

We are adapting three different analytical techniques to thermonuclear experiments. The first of these techniques gives solutions to the boundary-value problem in the form of an integral that can be numerically evaluated. These solutions are very accurate and can be calculated in a few seconds on a small digital computer. The disadvantage of this technique is that it can be applied only to regular geometries, such as coils above or between multiple planar conductors, coils in the presence of multiple cylindrical conductors, and coils in the presence of multiple spherical shells. These geometries are illustrated in Fig. 4.7.

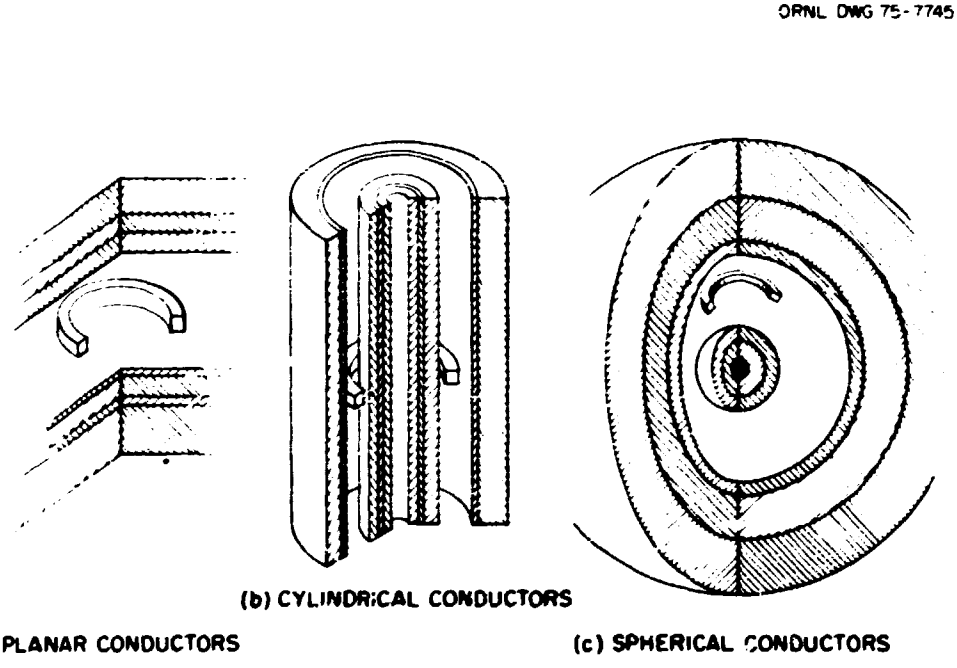


Fig. 4.7. Summary of the Type of Cases That Have Been Solved by Boundary-Value Techniques.

In order to solve for any phenomen other than induced voltages, the coils must be located on an axis of symmetry. Computer programs have been written to calculate the induced voltage, eddy-current density, and total dissipated power for coils above planar conductors and coils coaxial with cylindrical conductors. Also, programs have been written for magnetic fields[6] and net force generated for coils above planar conductors. The equations have been derived for eddy-current density, force density, power density, induced voltages, and magnetic fields for all cases, but they have not been programmed for computer solution. The derivations are for a single frequency, but they can be extended to any current shape by a Fourier synthesis (although some care must be observed for force and power calculations). We can determine the voltages and currents in a system of coils when one or more coils are charged or dumped. The accuracies of results obtained with this technique are about 0.1% to 1%.

The second method is a relaxation or iteration technique. The entire problem is laid out on a two- or three-dimensional lattice of points. A finite-difference equation for the field (usually the vector potential) at each point in terms of the field at the neighboring points is derived from the differential equation. The field is calculated for every point in the lattice a number of times until its value converges to that predicted by the differential equation. The relaxation technique can be applied to a pulse in a time-sequential mode or to a number of single sinusoidal frequencies, and a Fourier synthesis performed. The latter method will allow more freedom in selecting the shape of the charge and discharge wave forms with a given amount of calculation. Although, this technique is very general, it requires a large amount of memory and computation time, and the results are accurate only to within about 10%. We have derived equations for, programmed, and run two-dimensional relaxations, and have derived the equations for several different three-dimensional relaxations, but haven't programmed these. At present, we are trying to determine the optimum three-dimensional relaxation that will give the most accuracy with the least cost.

---

[6]C. V. Dodd and W. E. Deeds, *Calculation of Magnetic Fields from Time-Varying Currents in the Presence of Conductors*, ORNL-TM-4958 (July 1975).

The third method of determining the eddy-current effects is to measure them, using a model, with scaling applied to the apparatus size, the coil turns, the current and frequencies in the coils, and the size and electrical conductivity of the metals. In this technique, we may use either current pulses or discrete sinusoidal currents with a Fourier synthesis to obtain the pulses. The scaling relations have been derived, and several experiments have been performed to verify them.[7] We are also attempting to estimate the errors in extending the scaling to ferromagnetic materials.

The three techniques are complementary, and their applications may overlap in many areas. In these regions of overlap, we have errors ranging from about 0.5% for the numerical integrations compared with the models to about 10% for the relaxation calculations. These methods should be as valuable in designing thermonuclear experiments as they have been in designing nondestructive tests.

---

[7]C. V. Dodd and W. E. Deeds, *Scaling Relations for Eddy-Current Phenomena*, ORNL-5077 (in preparation).

# 5. EPR DESIGN SUPPORT

A. J. Moorhead J. L. Scott F. W. Wiffen

Materials for use in CTR systems must be chosen to provide maximum reliability of the reactor while providing minimum restriction on the reactor design and operation. For the EPR, these requirements and the tentative project schedule dictate that where possible materials must be chosed from those that are available now and have well understood properties under the proposed operating conditions. Although a large number of material selections must be made before detailed design can begin, only the two critical choices of the first structural wall and the plasma-structure interface (first radiation wall) have been considered in detail in establishing a references design for the EPR.

The first structural wall of the reference design is type 316 stainless steel. This material is available, economical, and adequate to meet the needs of EPR.

The first radiation wall presents a more difficult material choice. While it appears likely that a bare type 316 stainless steel is not the optimum plasma-structure interface, the properties required by the interface material are not well defined. A very tentative choice has been made for the reference design, a "shingle" wall, with the shingles held in place by a refractory metal lattice attached to the first structural wall. Possible candidate shingle materials include W, Nb, C, refractory carbides, and refractory oxides. Further design work will be required to verify the concept, and additional materials work will be necessary before the shingle material can be chosen.

Elaboration on the choice of type 316 stainless steel for the reference design first structural wall and of the considerations involved in selecting a first radiation wall are given in the following sections.

## 5.1 FIRST STRUCTURAL WALL FOR THE EPR REFERENCE DESIGN

The reference design material choice for the EPR first structural wall is type 316 stainless steel. This material is readily available, is economical, has a history of use and testing under conditions similar to

BLANK PAGE

those required for EPR, and will permit design, construction, and operation of EPR without unduly limiting the project goals.

Type 316 stainless steel is a readily available commercial product produced in a variety of forms needed for EPR construction. There is extensive experience in fabricating and welding this material, although of course procedures for this particular application may require some development. Design methods have been developed, and most of the data for design are available, but with limited experience in the higher temperature (creep-controlled) regime.

Requirements unique to CTR application of structural materials are resistance to the neutron flux originating from the D-T fusion and compatibility with blanket and coolant fluids. Nonneutronic radiation effects (surface radiation of photons, ions, and neutrals) are limited to surfaces facing the plasma and in the reference design are borne by the first radiation wall, which protects the first structural wall. Swelling from the neutron-produced displacement damage and helium will not be a problem for the modest effective full-power lifetime required of the EPR. However a more important effect of the neutron irradiation will set a limit on the type 316 stainless steel structure. Helium produced by $(n,\alpha)$ reactions will accumulate at the rate of 40 at. ppm per year of operation at a neutronic wall loading of 0.2 $MW/m^2$ and 100% plant factor. Helium in this concentration, or higher, will embrittle stainless steel in tensile loading at 600°C or higher[1] and dictate that the structure service temperature be held to no greater than 550°C.

Compatibility between the structural wall and lithium contained in blanket modules for tritium production also requires temperatures below 600°C. For a rapidly circulating lithium stream the required upper temperature limit would be approximately 500°C, but for the slow lithium circulation in the reference design a temperature limit of 550°C will probably be acceptable. In blanket segments designed only for heat generation (90% of the EPR blanket modules) the lithium will be replaced

---

[1]E. E. Bloom and F. W. Wiffen, *The Effects of Large Concentrations of Helium on the Mechanical Properties of Neutron-Irradiated Stainless Steel,* ORNL-TM-4861 (May 1975).

by potassium (sodium or NaK could also be used), and higher temperature limits could be tolerated from compatibility considerations with these liquid metals. The radiation embrittlement limitation of 550°C will, of course, still prevail.

Coolant tubes circulating helium through the blanket are subject to the same consideration on the lithium or potassium side. However, there are no problems anticipated at the interface inside the tube.

In summary, type 316 stainless steel will be an acceptable and adequate first structural wall material for the EPR, if temperatures are restricted to about 550°C, and this choice allows some optimism for extrapolation to higher power reactor systems (such as the demonstration reactor and beyond). Improvements in the performance of this alloy can probably be expected. Two approaches currently being examined are use of the material in the cold-worked state and use of the alloy with slight composition modification. Both these options promise improvement in the critical area of control of helium embrittlement.

## 5.2 THE FIRST RADIATION WALL FOR THE EPR REFERENCE DESIGN

### 5.2.1 The Plasma Contamination Problem

A first radiation wall is specified for the EPR, between the plasma and the first structural wall, because it is possible that bare type 316 stainless steel is not sufficiently resistant to the plasma environment. This environment of x rays, photons, ions, and neutral particles (with an aggregate energy deposition rate on the first wall of about 10 $W/cm^2$) and possibly the neutron flux will sputter the wall material into the plasma. The introduction of these impurities leads to radiation losses, which cool the plasma. Therefore, it is imperative that these impurities be kept to a minimum. As the energy losses are proportional to $Z^n$, where $Z$ is the atomic number and $n$ is between 2 and 4, the first radiation wall should preferably consist of a low-$Z$ material with a low sputtering rate.

### 5.2.2 Reference Design Choice

The reference liner consists of a refractory metal lattice supported from the first structural wall containing "shingles" of liner material.

Because cooling occurs by radiation alone, the temperatures well above 1000°C limit the materials selection to high-melting-point, nonvolatile materials.

The choice of shingle materials cannot yet be made, but some important materials considerations limit the choice. Sputtering coefficients for various elements exposed to helium ions with energies up to 600 eV are available.[2] The components of stainless steel — Fe, Ni, and Cr — have relatively high sputtering coefficients and relatively high Z's. The higher Z refractory metals have lower sputtering coefficients. Of the three low-Z solids — Be, B, and C — beryllium has a very high sputtering coefficient and boron is not compatible with the neutron spectrum, so a great deal of attention has focused on carbon. Until recently, it was thought that carbon was not susceptible to neutron radiation damage above 1200°C. However, data of Van Den Berg et al.[3] showed that graphites are more susceptible to neutron damage at higher temperatures and undergo rapid densification followed by expansion at fluences of interest to the EPR. With any form of carbon, one is also concerned about chemical reactions with energetic deuterium or tritium ions to form the equivalent of acetylene.

A possible alternative to carbon, SiC, has been proposed by Hopkins.[4] Silicon carbide has a relatively low Z and has better radiation stability than carbon. Not enough is known about hot-ion chemistry to know whether of not SiC will react with energetic deuterium or tritium ions.

The sputtering coefficients for various elements[2] suggest that some high-Z materials, such as tungsten, won't sputter enough to create problems.

---

[2]H. K. Perkins, *Ion and Fast Neutral Bombardment of Surfaces in Controlled Fusion Devices,* MATT-1005 (October 1973).

[3]M. Van Den Berg, M. R. Everett, and A. Kingsbury, "The Relationship Between Irradiation Temperature and Dimensional Changes of Nuclear Graphites," pp. 307–10 in *12th Biennial Conference on Carbon Extended Abstracts and Program,* (Held July 28–August 1, 1975 at Pittsburgh, Pa.), American Carbon Society.

[4]G. R. Hopkins, "Fusion Reactor Applications of Silicon Carbide and Carbon," pp. 437–47 in *Proceedings of the First Topical Meeting on the Technology of Controlled Nuclear Fusion,* San Diego, California, April 16–18, 1974, CONF-740402-P2.

Also, compounds such as WC, NbC, or ZrC might be better than any elemental material.

The choice of shingle materials then includes at least W, Nb, C, SiC, ZrC, NbC, WC, or some other refractory ceramic. Perhaps an oxide such as $Al_2O_3$ might be used. The final selection will be made on the basis of results of an experimental program, which assesses sputtering rates, neutron radiation effects, thermal-shock resistance, chemical sputtering, and other relevant properties at the temperature to be experienced in EPR.

### 5.2.3 Alternate Radiation Walls

One possible alternative is to coat the structural wall. Perhaps a coating would be preferable to "shingles". While extensive work has not been done on coatings, potential problem areas are fabrication difficulties, mismatch in thermal-expansion coefficients, lack of compatibility with the structural wall, thermal-shock resistance, and a number of others.

Another alternative is either the thin carbon curtain or the thick carbon liner proposed by Conn et al.[5] The potential problem areas with carbon were discussed above.

Another alternate geometry that we considered was honeycomb structures, brazed or otherwise attached to the structural wall. At present, not enough is known about honeycomb designs or materials to allow one to choose them for a reference design.

It is clear that a great deal of work remains to be done before a definitive and defensible choice of a first radiation wall can be made. Input to this problem area will be forthcoming from the surface studies program sponsored by DCTR and from the research program for the Impurities Study Experiment (ISX).

---

[5]R. W. Conn et al., "New Concepts for Controlled Fusion Reactor Blanket Design," *Nucl. Technol.* 26(2): 125–45 (June 1975).

# 6. THE INFLUENCE OF STRUCTURAL MATERIALS ON FUSION-REACTOR-BLANKET RESPONSE[1]

M. L. Williams R. T. Santoro T. A. Gabriel

The performance of fusion reactors, as well as the solution of problems concomitant with their operation and maintenance, will be influenced by the selection of structural material. In this contribution, the effects on nuclear response functionals (e.g., tritium-breeding ratio, energy deposition, absorbed dose during operation, material activation, activation dose after shutdown, and radiation damage) are calculated when niobium, type 304 stainless steel, and Nimonic 105 are considered as the structural materials in the ORNL conceptual reactor design.[1] The results differ from the earlier work of Steiner,[2] Price,[3] and Conn, Sung, and Abdou,[4] principally in the choice of materials and in the use of more recent nuclear data.

Transport calculations were performed with the discrete ordinates code[5] ANISN, using a P-3 scattering expansion, an S-12 quadrature, and the coupled neutron-gamma (100 $n$, 21 $\gamma$) cross-section library of Plaster, Santoro, and Ford.[6] Neutron and gamma-ray kerma factors for computing

---

[1]Contribution from the Neutron Physics Division.

[2]D. Steiner, "The Nuclear Performance of Vanadium as a Structural Material in Fusion Reactor Blankets," *Nucl. Fusion* 14: 33–44 (1974).

[3]W. G. Price, Jr., "Activation Hazards from Fusion Neutrons," pp. 217–21 in *Proc. Fifth Symp. Engineering Problems of Fusion Research (held Nov. 5–9, 1973, Princeton University, Princeton, N.J.)* IEEE Publ. No. 73 CHO 843-3-NPS, CONF-731114, Institute of Electrical and Electronics Engineers, New York, 1974.

[4]R. W. Conn, T. Y. Sung, and M. A. Abdou, *Comparative Study of Radioactivity and Afterheat in Several Fusion Reactor Blanket Designs*, FDM-113, University of Wisconsin (1974).

[5]W. W. Engle, Jr., *A Users Manual for ANISN: A One-Dimensional Discrete Ordinates Transport Code with Anisotropic Scattering*, K-1693 (Mar. 30, 1967).

[6]D. M. Plaster, R. T. Santoro, and W. E. Ford, III, *Coupled 100-Group Neutron and 21-Group Gamma-Ray Cross Sections for FPR Calculations*, ORNL-TM-4872 (April 1975).

BLANK PAGE

the energy deposition were generated by MACKLIB[7] and SMUG,[8] respectively. Activation cross sections were obtained from ENDF/B-4 and from the compilation of Muir,[9] and displacement cross sections were taken from the work of Gabriel, Amburgey, and Greene.[10] Blanket responses were calculated by changing structure cross sections and holding other parameters constant to obtain energy-dependent fluxes as functions of structural material. These values were then substituted into the appropriate functionals to evaluate the desired responses.

A summary of nuclear responses as functions of the selected materials for continuous operation with a wall loading of 1 $MW/m^2$ is given in Table 6.1. The lower breeding ratio with Nimonic 105 structure is due to high parasitic absorption in nickel and cobalt. The absorbed dose at the outer wall during operation is highest with Nimonic because of secondary gamma rays from cobalt. The activation dose is high for all materials, but values will be reduced when conditions other than continuous operation are assumed.

The first-wall activation after one year of continuous operation at 1 $MW/m^2$ is shown in Fig. 6.1 as a function of time after shutdown. The niobium activity is dominated at early times by $^{92m}Nb$ ($t_{1/2}$ = 10.1 days) and at later times by $^{93m}Nb$ ($t_{1/2}$ = 3.7 years). Stainless steel activity follows the decay of $^{54}Mn$ ($t_{1/2}$ = 313 days) and $^{55}Fe$ ($t_{1/2}$ = 2.4 years), while Nimonic 105 activity depends mostly on $^{58}Co$ (71.4 days) and $^{60}Co$ (5.3 years).

---

[7]M. A. Abdou and R. W. Roussin, *MACKLIB — 100-Group Neutron Fluence-to-Kerma Factors and Reaction Cross Sections Generated by the MACK Computer Program from Data in ENDF Format*, ORNL-TM-3995 (August 1974).

[8]N. M. Greene et al., *AMPX: A Modular Code System for Generating Coupled Multigroup Neutron-Gamma Libraries from ENDF/B*, ORNL-TM-3706 (in press).

[9]D. W. Muir, *Data Library MONTAGE*, DLC-33 (1975).

[10]T. A. Gabriel, J. D. Amburgey, and N. M. Greene, "Recoil Spectra, Damage Energy, and Displacement Cross Sections," *Trans. Am. Nucl. Soc.* 21: 67 (1975).

Table 6.1. Comparison of the Blanket Response as a Function of Structural Material

| Response | Structural Material | | |
|---|---|---|---|
| | Nb[a] | 304 SS[b] | Nimonic-105[c] |
| Tritium breeding ratio | 1.52 | 1.53 | 1.46 |
| Operating absorbed dose at the outer wall, rad/hr | $1.75 \times 10^7$ | $1.74 \times 10^7$ | $2.21 \times 10^7$ |
| First-wall heating, kW/cm of circumference | 3.05 | 4.42 | 5.19 |
| First-wall damage, dpa | 12.84 | 10.80 | 16.89 |
| Afterheat at shutdown, W/cm of circumference | 386 | 79.3 | 522 |
| Absorbed dose at one day after shutdown,[d] rad/hr | $5.76 \times 10^6$ | $1.02 \times 10^6$ | $5.38 \times 10^6$ |
| First-wall activation at shutdown,[d] dis $sec^{-1}$ $cm^{-3}$ | $7.99 \times 10^{12}$ | $2.29 \times 10^{12}$ | $6.61 \times 10^{12}$ |

[a] 100% $^{93}$Nb.

[b] 70.5% Fe, 19.0% Cr, 9.0% Ni, and 1.5% Mn.

[c] 54.2% Ni, 20.0% Co, 15.0% Cr, 5.0% Mo, 4.5% Al, and 1.3% Ti.

[d] For continuous operation for one year at 1 $MW/m^2$.

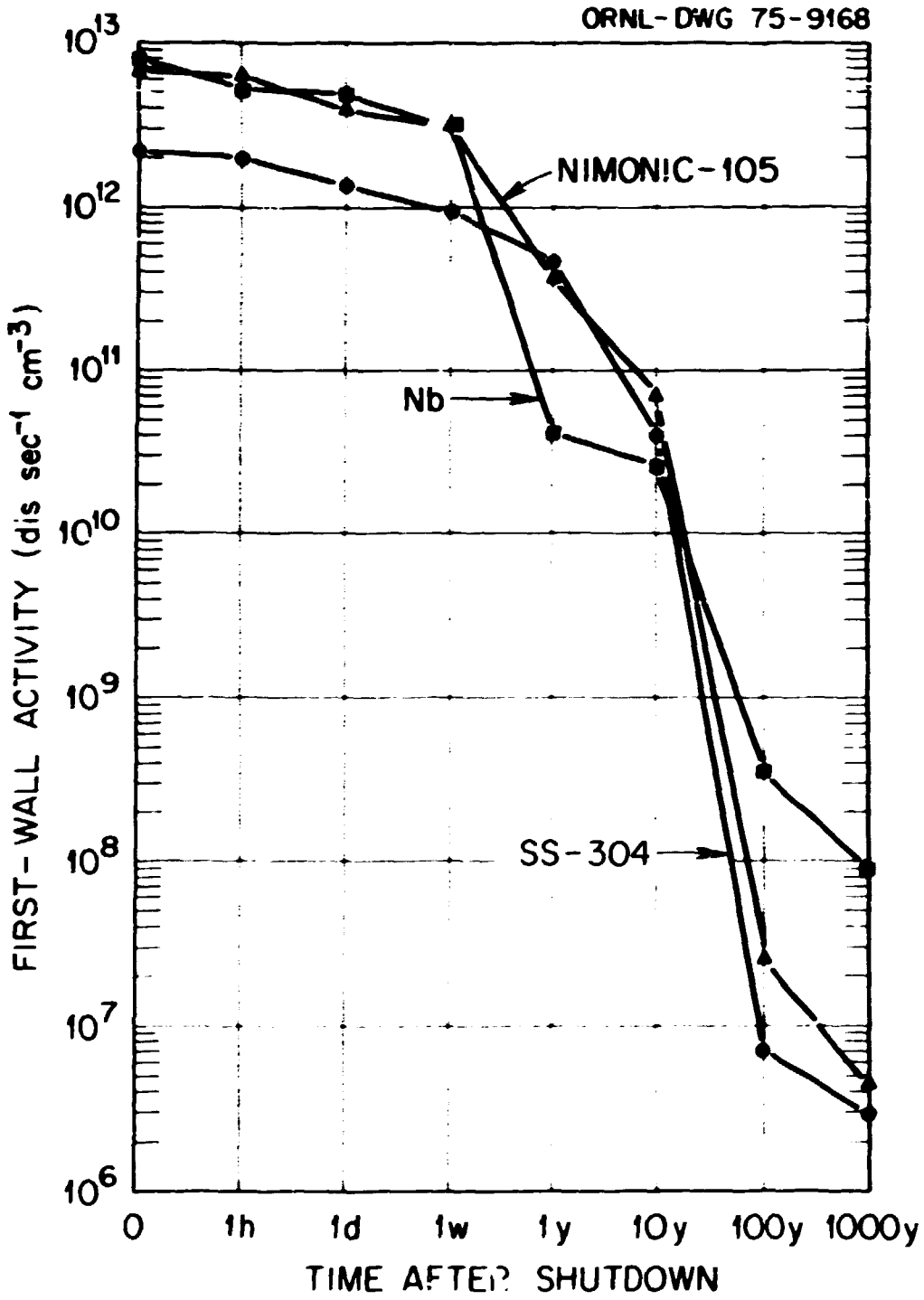


Fig. 6.1. First-Wall Activity as a Function of Time After Shutdown for One Year of Continuous Operation at 1 MW/m$^2$.